catalysts

MDPI

Review

The Research Progress of Ruthenium-Based Catalysts for the Alkaline Hydrogen Evolution Reaction in Water Electrolysis

Bi-Li Lin [1], Xing Chen [2], Bai-Tong Niu [2], Yuan-Ting Lin [1], Yan-Xin Chen [3] and Xiu-Mei Lin [1,*]

[1] College of Chemistry, Chemical Engineering and Environment, Minnan Normal University, Zhangzhou 363000, China; linbili083107@163.com (B.-L.L.); linyuanting2024@163.com (Y.-T.L.)
[2] State Key Laboratory of Physical Chemistry of Solid Surfaces, College of Chemistry and Chemical Engineering, Xiamen University, Xiamen 361005, China; xchenfzu@163.com (X.C.); baitongniu@163.com (B.-T.N.)
[3] State Key Laboratory of Structural Chemistry, Fujian Institute of Research on the Structure of Matter, Chinese Academy of Sciences, Fuzhou 350002, China; yanxinchen@fjirsm.ac.cn
* Correspondence: xiu-mei.lin@xmu.edu.cn

Abstract: The performance of the cathodic hydrogen evolution reaction (HER) in alkaline water electrolysis, an attractive hydrogen production technology, is highly dependent on efficient catalysts. Ruthenium (Ru), which is more affordable than platinum (Pt) and has a metal–hydrogen bond strength comparable to that of Pt, shows exceptional catalytic activity for the alkaline HER. Consequently, in recent years, research in the field of hydrogen production through alkaline water electrolysis has increasingly focused on Ru as a key element. This review first discusses the fundamentals of the alkaline HER, including principles, factors affecting its performance, and regulation strategies for its performance improvement. The research progress of ruthenium-based catalysts for the alkaline HER is then summarized with selected examples. The electronic structures of various ruthenium nanoparticles, ruthenium-M (M = noble metals and transition metals) heterogeneous catalysts, and ruthenium-based compounds are regulated by modulating the components and ligands of Ru atoms, aiming to achieve low water dissociation energies and optimal binding energies for hydrogen (H) and hydroxyl (−OH) groups, thereby enhancing the alkaline HER catalytic performance. Finally, the problems, challenges, and future development directions of the alkaline HER are proposed.

Keywords: ruthenium-based catalysts; alkaline hydrogen evolution reaction; water electrolysis; electronic structure; components and ligands modulation

check for updates

Citation: Lin, B.-L.; Chen, X.; Niu, B.-T.; Lin, Y.-T.; Chen, Y.-X.; Lin, X.-M. The Research Progress of Ruthenium-Based Catalysts for the Alkaline Hydrogen Evolution Reaction in Water Electrolysis. *Catalysts* **2024**, *14*, 671. https://doi.org/10.3390/catal14100671

Academic Editor: Sang-Il Choi

Received: 2 September 2024
Revised: 20 September 2024
Accepted: 26 September 2024
Published: 28 September 2024

Copyright: © 2024 by the authors. Licensee MDPI, Basel, Switzerland. This article is an open access article distributed under the terms and conditions of the Creative Commons Attribution (CC BY) license (https://creativecommons.org/licenses/by/4.0/).

1. Introduction

Energy production and storage represent a crucial foundation for the survival and development of human society. The daily accelerated pace of social development has precipitated a surge in traditional fossil fuel consumption, causing an energy crisis and environmental degradation [1–4]. There is an urgent necessity to develop a sustainable green energy source that could promote future human development. Hydrogen offers several advantages, including a high calorific value of combustion, pure and non-polluting products, and abundant resources, which makes it the optimal alternative to non-renewable energy sources [5,6]. In terms of market share, the existing industrial techniques for producing hydrogen are steam methane reforming, coal gasification, and water electrolysis [7,8]. The dominant approaches to hydrogen production are the first two methods. However, they are associated with significant drawbacks, including a low conversion rate and considerable environmental contamination. Coupling these methods with the electricity produced by renewable energy like solar or wind to perform water electrolysis (Figure 1a) for hydrogen generation is one of the most effective pathways to develop clean hydrogen energy. The implementation of water electrolysis for hydrogen production is an efficient pathway for

clean hydrogen energy. This approach lowers greenhouse gas emissions and decreases the dependence on fossil fuels, working toward an eco-friendly energy future.

Alkaline water electrolysis has become the most prevalent technology for hydrogen production in the industry largely due to its straightforward operational convenience, relatively low equipment costs, and extended lifespan [9]. However, the generation of hydrogen from alkaline water electrolysis necessitates the use of robust catalysts to facilitate the kinetically slow water dissociation and, consequently, to enhance the reaction kinetics [10]. Thus, the focus of research on the alkaline HER is the development of efficient catalysts to reduce energy consumption while improving economic efficiency. The noble metals platinum (Pt) and iridium (Ir) possess excellent alkaline HER catalytic performance. However, their scarcity and expensive price restrict their large-scale application [11,12]. Following the Sabatier principle [13], Pt is deemed to possess the optimal bond strength of metal–hydrogen, thereby exhibiting the most efficacious HER performance. Nevertheless, this principle is inadequate for explaining the observation that the HER activity of Pt in alkaline media is 2–3 orders of magnitude lower than that observed in acidic media. [14]. It has been demonstrated that the generation of hydrogen in alkaline media necessitates the surmounting of an additional energy barrier for water dissociation compared to that in acidic media, which represents a pivotal factor limiting the HER kinetics of Pt-based catalysts under alkaline conditions [15]. It is, therefore, imperative to develop cost-effective catalysts with high HER performance in alkaline media. The price of Ru is only one-quarter that of Pt [16], while it displays high water dissociation and hydroxy chemisorption capability. Lots of Ru-based catalysts have been observed to exhibit enhanced HER performance in alkaline media compared to Pt [17]. Consequently, Ru-based catalysts have attracted significant attention in alkaline HER research in recent years.

Despite Ru-based catalysts demonstrating considerable promise in the alkaline HER, their fundamental investigations and industrial applications are still in the initial stage. There remains a considerable opportunity and potential for the improvement of the alkaline HER performance of Ru-based catalysts. Consequently, in this paper, the research progress of Ru-based catalysts for the alkaline HER is summarized with selected examples to reveal the structure–performance relationship to guide the design and development of highly effective Ru-based catalysts with superior performance.

2. Mechanism of Alkaline HER

The cathodic reaction in water electrolysis is a process that can be divided into three fundamental stages, i.e., the Volmer, Heyrovsky, and Tafel processes. The mechanism of the HER in alkaline media [18] is illustrated in the diagram below:

$$\text{Volmer: } H_2O + e + {}^{-}* \rightarrow H^* + OH^- \quad (1)$$

$$\text{Heyrovsky: } H^* + H_2O + e^- \rightarrow H_2 + OH + {}^{-}* \quad (2)$$

$$\text{Tafel: } H^* + H^* \rightarrow H_2 + 2^* \quad (3)$$

where H* represents the electrochemically adsorbed hydrogen atom, and * represents the active site. By calculating the Tafel slope, the HER process can be assigned to either a Volmer–Tafel or Volmer–Heyrovsky pathway [19,20]. In alkaline conditions, the formation of H* requires additional energy to facilitate the initial water dissociation, leading to sluggish alkaline HER kinetics, which is typically 2–3 orders of magnitude slower than in acidic media due to the significant energy barrier for water dissociation [21]. Nevertheless, the stability and corrosion issues associated with catalysts and reaction devices are significant challenges that cannot be circumvented in acidic media. As a result, there is a pressing need to improve water dissociation kinetics, making it a central focus of current alkaline water electrolysis research.

3. Factors Affecting the Alkaline HER Performance of Ru-Based Catalysts and the Related Regulation Strategies

According to the mechanism outlined above, although the HER solely produces H_2, it encompasses several reaction steps, specifically, adsorption, activation, and desorption. In alkaline media, in addition to the steps of H* binding and H_2 formation, the processes of H_2O adsorption, activation, dissociation, and -OH transportation are all significantly affected by the properties of Ru-based catalysts. Optimizing the binding energy of reaction intermediates with Ru-based catalyst surfaces is critical for catalyst design and performance improvement. The optimization methods include regulating the composition, structure, or surface properties of the catalyst to create more appropriate active sites for intermediates as well as regulating the surface coverage of the intermediates and minimizing the competitive response (e.g., desorption or peroxidation).

3.1. Regulation of H Adsorption Free Energy (ΔG_H) on Ru-Based Catalyst Surfaces*

The formation and desorption of H^* are of pivotal importance to the understanding of the kinetics and mechanism of the HER. The adsorption and desorption capability of H^* on catalyst surfaces could be assessed by calculating ΔG_H* using density functional theory (DFT) [22]. As illustrated in Figure 1b, Pt is in the center of the volcano plot of the hydrogen adsorption free energy, indicating the optimal M-H binding energy (M stands for metal) [23], and thus has an unparalleled performance of hydrogen evolution in an acidic electrolyte. Experimental findings and DFT calculations [22,23] show that the M-H binding energy of Ru is somewhat less pronounced than that of Pt, leading to the inferior acidic HER performance of Ru than Pt.

The outer electron configuration of Pt is $[Xe]4f^{14}\ 5d^9\ 6s^1$, and that of Ru is $[Kr]4d^7\ 5s^1$; therefore, Pt has two unpaired electrons within the outermost stratum, while Ru has four unpaired electrons. This difference results in a higher empty orbit density above the Fermi energy level (E_f) of Ru than Pt. Consequently, the adsorption of reaction intermediates on Ru surfaces is stronger than that on Pt surfaces during the catalytic reaction processes. These hypotheses are further confirmed by the d-band centers on the surfaces of face-centered cubic (fcc) Pt (111) and hexagonal close-packed (hcp) lattice Ru (0001), which are the most stable surfaces of Pt and Ru, respectively. The d-band centers of Pt are about −2.2 eV [24], while the Ru is −1.41 eV [25], which explains the stronger adsorption of Ru to the reaction intermediates than Pt. To make Ru behave like Pt in the H adsorption, electrons can be inserted into Ru's empty orbitals to weaken the Ru-H bond and promote the desorption of H* [24–26]. In light of the aforementioned conclusions, a variety of strategies can be employed to control the ΔG_H* and enhance the HER performance, including combination with carriers, alloying, doping, the construction of heterostructures, etc. [27–32].

3.2. Regulation of H_2O Adsorption and Activation on Ru-Based Catalyst Surfaces

It has been reported that the energy barrier of H_2O dissociation is greater than that of H_2 desorption and is the rate-limiting step in the alkaline HER. Generally, the O-H bond is more likely to be cleaved when the H_2O molecules are more strongly adsorbed on the active sites of catalyst surfaces due to the strong electronic interactions between H_2O and active sites, which weaken the electronic interactions within the O-H bond and facilitate bond cleavage [33]. In most cases, the adsorption of H_2O on the active sites of transition metal catalyst surfaces is through the coordination between the empty orbit of the metal and the lone electrons pair of O. Consequently, the abundance and variety of empty orbits of the catalyst that can coordinate with H_2O are vital for water adsorption and dissociation. This information provides an important foundation for the rational design of H_2O adsorption/activation sites on alkaline HER catalyst surfaces. Great effort has been made to improve the adsorption and dissociation of H_2O and the incorporation of transition metals onto catalyst surfaces is a productive strategy, showing prominent potential for the alkaline HER.

3.3. Regulation of Adsorption and Coverage of -OH Species on Ru-Based Catalyst Surfaces

The design of HER catalysts is primarily based on their intrinsic interactions with H_2O and H^* species, while the adsorption and desorption of −OH species on catalyst surfaces are usually neglected. Ru has a good water dissociation capability and a strong −OH species adsorption capability as well. The substantial binding energy between the active sites of catalyst surfaces and the −OH species restricts the transfer of −OH species and inhibits the overall alkaline HER activity [34,35]. Accordingly, the design of alkaline HER catalysts to relieve the strong adsorption between active sites and −OH species is crucial for the alkaline HER. The −OH species adsorption and desorption processes involve the Volmer and Heyrovsky steps of the alkaline HER, which can be modulated using transition metals with different oxygen affinities. Therefore, designing Ru-based compound catalysts with multifunctional components (metal Ru and transition metal oxides) to modulate the interactions between the catalysts and all relevant adsorbates (H_2O, H*, and −OH species) simultaneously can synergistically improve reaction kinetics for the efficient alkaline HER.

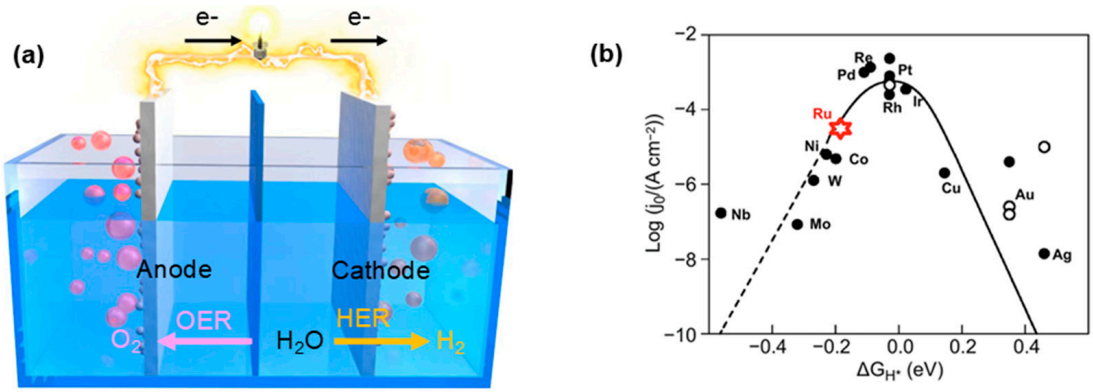


Figure 1. (**a**) A diagram of the water electrolysis process. (**b**) The HER Volcano plot for various metals against the ΔG_{Hads}. Reproduced with permission from the authors of [23]. Copyright © 2021 Springer Nature.

4. Research Progress of Ru-Based Catalysts in the Alkaline HER

To overcome the slow kinetics in the alkaline HER, highly efficient Ru-based catalysts should follow the following principles: low hydrolysis ionization energy and adequate binding energy of H and −OH. Ru nanoparticle catalysts of a single component usually satisfy these principles by modulating the morphology, size, and interaction with the carriers; however, it is challenging for single-component catalysts to fulfill these intrinsic functional requirements simultaneously, which could be achieved by heterogeneous and composite catalysts consisting of different functional components that can favor the alkaline HER process. In the following sections, we will summarize the research progress of Ru-based catalysts in the alkaline HER with selected examples, focusing on both metallic ruthenium and various ruthenium-based compounds.

4.1. Ruthenium Nanoparticles

Ruthenium nanoparticles (NPs) can greatly increase the atomic utilization of Ru compared to Ru bulk materials. Anchoring Ru atoms to specific carriers and modulating the electronic structure by altering the metal (Ru)–carrier interactions [36] can also accelerate the dissociation of water and optimize the adsorption and desorption of H. Ideal carriers usually possess the following properties: a high surface area to expose more active sites, substantial metal–carrier bonding for the uniform dispersion of Ru NPs, good electrical conductivity to accelerate electron transport, and excellent corrosion resistance in the electrolyte [30,37]. Therefore, ordered porous materials including carbon nanomaterials (carbon nanorods, carbon nanotubes, etc.) [26,38,39] and crystalline porous materials (metal-organic frameworks (MOFs) [40,41], covalent organic frameworks (COFs) [42], etc.) are

generally used. Ma et al. [26] synthesized hollow mesoporous carbon spheres that confined Ru NPs (Ru/HMCs-500) by embedding Ru nanoparticles on the pores of porous carbon spheres and found that the pore confinement, high dispersibility, and anchoring effect ensured high catalytic activity and stability. The Ru/HMCs-500 showed seven times higher mass activity than that of Pt/C (1606.9 mA mg^{-1} vs. 228.2 mA·mg^{-1}) and good stability with a test time of 12 h after 2000 cyclic voltammetry (CV) cycles in alkaline media. Thalluri et al. [43] deposited 100 cycles of atomic layer Ru on carbon paper (CP100C Ru), in which the nucleation of Ru was restrained by enhancing the carbonyl (C=O) functionality on carbon paper and finally allowed the uniform deposition of ruthenium, thus increasing the specific surface and active sites of catalysts and optimizing the HER performance. In the alkaline HER, the CP100C Ru had a low overpotential of 4.7 mV at −10 mA·cm^{-2}, a high turnover frequency (TOF) of 1.92 H_2 s^{-1} at 30 mV, and good stability. Li et al. [44] fabricated Ru/C with different particle sizes at different temperatures using the reduction–impregnation method, which efficiently regulated the adsorption of H_2 and -OH on Ru NPs. Researchers found that the particle size of Ru increased with increasing treatment temperature, among which Ru/C-600 (the size of the Ru particle is 6 nm) showed the best alkaline HER performance, with an overpotential of 30 mV at −10 mA·cm^{-2} and a Tafel slope of 33.7 mV·dec^{-1}.

The introduction of heteroatoms (Boron (B), Nitrogen (N), Phosphorus (P), and Sulfur (S)) into the carbon carriers can alter the ligand environment and further change the electronic structure of Ru atoms, hence improving the catalytic performance of Ru. The d-band center of metal catalysts is intimately associated with its binding energy of H atoms. The interaction of Ru nanoclusters (NCs) with N-doped carbon carriers results in the decline of the d-band center and the weakening of H adsorption, leading to the optimization of alkaline HER performance. Huang et al. [31] loaded Ru NCs on porous N-doped carbon (Ru NCs/NC), which had an overpotential of 14 mV at −10 mA·cm^{-2} and showed only a slight voltage change after an alkaline HER for 50 h. Ye et al. [38] anchored Ru NCs on a B/N-doped graphene (Ru NCs/BNG) catalyst shown in Figure 2a, which lowered the threshold energy for H_2 generation and altered the HER process by utilizing electronic interactions between B and Ru. The electrochemical impedance spectroscopy (EIS), shown in Figure 2b, of Ru NCs/BNG had good electrical conductivity, which led to the enhanced alkaline HER performance of having an overpotential of 14 mV at −10 mA·cm^{-2} (Figure 2c) and a Tafel slope of 28.9 mV·dec^{-1}. Zhao et al. [45] used the colloidal synthesis method to change the reaction temperature to obtain P-Ru nanoparticles (NPs) with different phosphorus doping contents to modulate the electronic structure of Ru. The optimization of the free energy of ruthenium-hydrogen (Ru-H) adsorption was achieved to increase the alkaline HER activity, among which the catalyst (P-Ru-3/C) synthesized at 320 °C showed the highest catalytic activity with an overpotential of 31 mV at −10 mA·cm^{-2} and a potential mass activity of 1.03 mA·$\mu g_{Ru}{}^{-1}$ at 50 mV.

Ajmal et al. [46] succeeded in making uniformly dispersed Ru nanoparticles by a pyrolysis method. The best performance catalyst Ru@N-P-C-800 was obtained on a nitrogen and phosphorus co-doped thin carbon substrate when the pyrolysis temperature was 800 °C. This method promoted the even distribution of Ru NPs on a carbon substrate, enhanced the electron transfer efficiency, and formed a collaborative effect, which led to the optimization of the alkaline HER performance of having an overpotential of 45 mV at −10 mA·cm^{-2} and a Tafel slope of 115 mV·dec^{-1}. Sun et al. [47] prepared Ru/S-rGO composites using a one-pot method, where the evolution and wide dispersion of ultrasmall Ru NPs could be obtained by sulfur doping and a moderate degree of oxidation, which increased the availability of active sites. Meanwhile, the metal–carrier interactions among Ru NPs and sulfur-doped graphene led to a decline in the electron density of Ru, which promoted the breakage of the H-OH bond, resulting in improved alkaline HER performance with a minimum overpotential of 14 mV at 20 mA·cm^{-2}. Furthermore, the double-layer capacitance (C_{dl}) value of Ru/S-rGO was 49.0 mF·cm^{-2}. Li et al. [39] anchored sulfur-liganded Ru NCs to nitrogen-sulfur co-doped carbon nanosheets via space-confined

pyrolyzed sheets to obtain Ru-S/N-C, and the kinetics of the HER reaction was accelerated through an interfacial charge transfer from the cooperative electronic connectivity among Ru, N, S, and C to Ru. The results show that Ru-S/N-C exhibited an overpotential of 10 mV at 10 mA·cm^{-2} and a superior TOF of 2.3 H_2 s^{-1} at 50 mV, as well as durable CV stability.

Crystalline porous materials are applicable candidates for the HER owing to their ordered frameworks, controllable synthesis, and viable functional enhancement. However, these materials have the disadvantages of weak reaction sites and poor electron mobility [48]. The modification of Ru onto the highly ordered porous frameworks as the catalytic center and the introduction of conductive carbon nanotubes are helpful for reactants to access the internal active center during H_2 production. He et al. [49] synthesized Ru-doped Co-catecholate (Co-CAT) in one step by using the solvent–thermal method to obtain the Ru-doped Co-catecholate loaded on carbon cloth (RuCo-CAT/CC) catalyst, which enhanced the electrical conductivity and promoted water dissociation and thus had an alkaline HER overpotential of only 38 mV at −10 mA·cm^{-2}, which was below the value of commercial Pt/C (45 mV) [50]. Li et al. [51] obtained CoRu-BPDC (BPDC: 4,4′-Biphenyldicarboxylic acid) by dispersing Ru atoms into the cobalt-based MOFs shown in Figure 2d. The special electronic structure formed helped to optimize the attaching strength of H*. The catalyst thus had an overpotential of 37 mV at −10 mA·cm^{-2} and can work stably for 300 and 120 h at −10 and −100 mA·cm^{-2}, as shown in Figure 2e. Sun et al. [52] grafted Ru-modified bipyridyl COF (TpBpy-Ru) onto carboxyl-functionalized carbon nanotubes (CNTs) to obtain c-CNT-0.68@TpBpy-Ru (in which 0.68 represents the mass ratio of the c-CNTs to COF monomers) and obtained an overpotential of 112 mV at −10 mA·cm^{-2} and stability of 12 h.

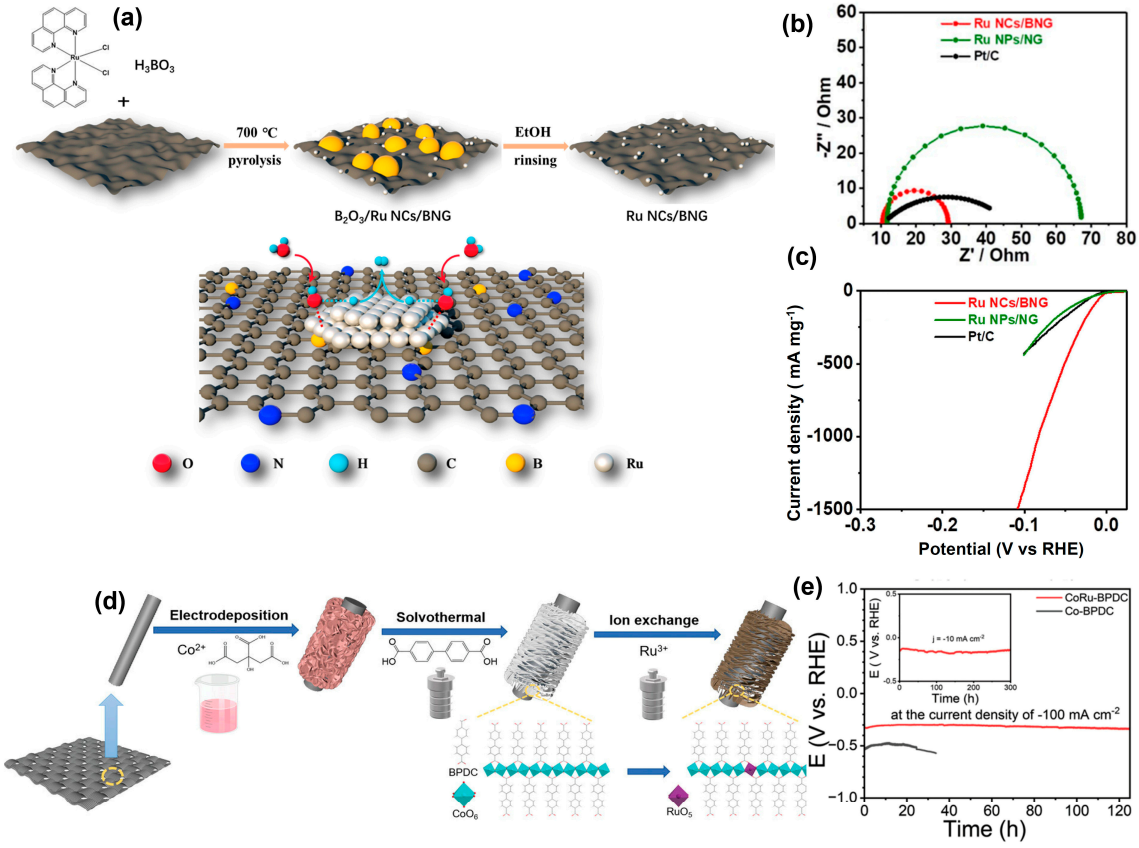


Figure 2. (**a**) A schematic illustration of the preparation of Ru NCs/BNG. (**b**) Nyquist plots of 50 mV and (**c**) LSV curves of Ru NCs/BNG, Ru NPs/NG, and Pt/C in 1 M KOH at 2 mV·s^{-1}. (**d**) The preparation and structure of the CoRu-BPDC/CC catalyst. (**e**) Chronopotentiometry curves of CoRu-BPDC/CC electrodes at −100 mA·cm^{-2} and −10 mA·cm^{-2} (inset in (**e**)). Reproduced with permission from the authors of [38,51]. Copyright © 2019 Elsevier Ltd. and 2023 Wiley-VCH GmbH.

4.2. Ruthenium-M Heterogeneous Catalysts (M = Noble Metals and Transition Metals)

It has been demonstrated that the combination of Ru with other metal elements to form heterogeneous catalysts can increase the density of active sites and form heteroatomic bonds to optimize the composition and electron configuration of the catalyst, which leads to the redistribution of charges and suitable binding energies with intermediate species, thus boosting HER performance [53,54]. Chen et al. [53] modified Pt onto highly dispersed Ru NPs by a cold plasma technique and obtained an excellent HER catalyst of Pt single atoms on Ru NPs with 0.47 wt% content of Pt loaded on the commercial acetylene black ($Pt_{0.47}$-Ru/Acet), as shown in Figure 3a. The catalyst showed excellent alkaline HER performance with a 17 mV overpotential at -10 mA·cm^{-2} (Figure 3b) and good stability after 8000 CV cycles, as shown in Figure 3c. Pang et al. [55] applied a liquid laser irradiation strategy to anchor isolated Pt atoms to the Ru host on surface-modified carbon nanotubes (PtRu/mCNTs) and modulated the d-band of Ru by increasing the alloying degree to enhance the performance. The PtRu/mCNTs displayed excellent activity and stability with an overpotential of 15 mV at -10 mA·cm^{-2} and a stable operation for up to 48 h at -10 mA·cm^{-2}. Li et al. [56] synthesized carbon-cloth-supported PtRu catalyst ($PtRu/CC_{1500}$) by an electrochemical deposition method, in which Pt atoms were bonded to the Ru substrate through Pt-Ru bonds. The formation of Pt-Ru bonds released additional free electrons for Pt atoms, which proficiently controlled the electronic structure of Ru and tuned the ΔG_H* close to zero to realize the good performance of having an overpotential of 19 mV at -10 mA·cm^{-2} and an outstanding mass current density of 198.7 mA·cm^{-2} at 109.9 mA·mg^{-1} (59 times superior to that of commercial Pt/C catalysts).

Although Ru showed good hydrolysis dissociation ability, OH* strongly bounded to Ru, resulting in the tendency of OH* poisoning on the active sites, which can be solved by doping Mo atoms to precisely modulate the electronic structure of Ru, thereby changing the association between Ru and OH*. Yang et al. [54] prepared a Mo-doped Ru nanocluster embedded on an N-doped carbon framework (RuMo/NC) catalyst with a Ru content of only 0.4 wt% by one-pot pyrolysis. The catalyst exhibited good catalytic activity with an overpotential of 24 mV at -10 mA·cm^{-2} and a Tafel slope of 52.8 mV·dec^{-1}. Li et al. [57] encapsulated phosphomolybdic acid (POM) in bimetallic MOFs, followed by thermal and etching treatments to combine P and Mo bis-doped ultrasmall Ru NCs into P-doped porous carbon (P-Mo-Ru@PC), which achieved a low overpotential of 21 mV at -10 mA·cm^{-2} and a low Tafel slope of 21.7 mV·dec^{-1}, and the mass activity of P-Mo-Ru@PC (1525 mA·mg^{-1}) was six times higher than that of Pt/C. The relatively high potential barrier for H_2O dissociation on the Ru surface limits the enhancement of the HER kinetics. The RuMo catalysts have a bi-site synergistic effect, allowing the simultaneous achievement of high activity and stability [58,59]. Chao et al. [60] used a wet impregnation method to synthesize Ru_1-Mo_2C NPs, as shown in Figure 3d. The water dissociated on Mo_2C and then the generated H atoms transferred to the adjacent Ru mono-site for the formation and desorption of H_2, achieving high alkaline HER activity and durability of an ultra-low overpotential of 10.8 mV at -10 mA·cm^{-2}, as shown in Figure 3e, and a stability for more than 200 h at 500 mA·cm^{-2}.

When Mo is incorporated into Ru at the atomic level, the charge is transferred from Mo to Ru due to the greater electronegativity of Ru, thus changing the electronic structure of Ru and improving the reactivity of the H_2 generation. Embedding metallic Mo atoms into Ru lattices creates highly active sites through spatial site resistance, resulting in high bifunctional activity. Okazoe et al. [61] used carbonyl complexes as precursors to synthesize MoRu solid-solution alloy NPs by thermal decomposition and achieved an overpotential of 27.1 mV at -15 mA·cm^{-2} and a low Tafel slope of 21.7 mV·dec^{-1}. Li et al. [62] synthesized Mo-Ru nanostructured alloys (NSAs) by a wet chemical method, in which 16 mV was sufficient to drive a current density of -10 mA·cm^{-2}, and stability for 250 h was kept. The robust interaction between Ru and Co reduced the energy barrier to hydrolysis, accelerated the formation of H^*, and optimized the adsorption of H_{ads} intermediates to achieve excellent HER activity at the Ru-Co interface [63]. In the alloy, Ru

atoms were fixed in the metallic matrix and coordinated symmetrically across the plane. Owing to the lack of symmetry in the *Z*-axis, the electrical charge migration between the metal substrate and Ru sites had a direct effect on the charge configuration of the 4 d_z^2 orbitals of Ru, which in turn affects the Ru-H binding strength and the HER performance. Cai et al. [64] utilized a rapid co-precipitation process and a mild electrochemical reduction technique to prepare RuCo alloy nanosheets (RuCo ANSs) comprising Ru atoms situated as isolated active sites in Co substrate. Figure 4a illustrates the schematic representation of the coupling of Ru $4dz^2$ with H 1s orbitals. RuCo possesses a planar symmetrical and *Z*-axis asymmetrical coordination framework, and the optimal $4d_z^2$ electronic structure is shown in Figure 4b. The associated optimized hydrogen binding energy is shown in Figure 4c, which leads to excellent properties of a 10 mV overpotential at -10 mA·cm^{-2}, as shown in Figure 4d, and a Tafel slope of 20.6 mV·dec^{-1}. Kutyła et al. [63] synthesized the Ru-Co@Ti_2AlC using an electrodeposition method and achieved overpotentials of 25 and 95 mV at 10 and -100 mA·cm^{-2}. Minimizing the size of nano-catalysts and creating ultra-tiny metal cluster-embedded materials are efficient strategies to enhance the electrochemical reaction and catalyst utilization. Yang et al. [65] produced amorphous Ru clusters generated on Co-doped hollow carbon nanocages (a-Ru@Co-DHC), which are rich in defects by an electrostatic spinning technique and showed the excellent alkaline HER performance of having a Tafel slope of 62 mV·dec^{-1}, an overpotential of 40 mV at -10 mA·cm^{-2}, and a high activity of 3.77 mA·$\mu g_{Ru}{}^{-1}$(@100 mV). Zhang et al. [66] obtained atomically dispersed Ru on cobalt nanoparticles on macro/microporous frameworks (M-Co NPs@Ru SAs/NC) by carbonization and an electrochemical substitution strategy. The powerful electronic effects among the bimetals and the unique macro-porous structure influenced the electronic structure of the molecules and shortened the transport distance of the molecules to achieve an overpotential of 34 mV at -10 mA·cm^{-2} and a TOF of 4284 H_2 at -0.05 V·s^{-1}.

Incorporating Ni with Ru can alter the pristine lattice structure of Ru by introducing electronic effects and structural modifications [67], leading to optimal binding energies of H* and OH* intermediates to the Ru active sites for fast kinetics of the Tafel step. Additionally, the abundance and affordability of Ni can effectively reduce the material cost [68], while maintaining or even improving the catalytic performance. Chen et al. [69] applied a high-temperature solid-phase method to fabricate ordered Ru-Ni, resulting in the optimal adsorption energy of H* and OH* intermediates on the Ru catalytic center due to the formation of ordered RuNi cores exerting uniform compression strain on the Ru interface. The catalyst accelerated the kinetics of the Tafel step and optimized the alkaline HER performance of having an overpotential of 23 mV, a Tafel slope of 25.9 mV·dec^{-1} at -10 mA·cm^{-2}, and a mass activity of 4.83 A·mg^{-1}. Wang et al. [70] obtained the Ru/Ni@C catalyst by anchoring Ru clusters (smaller than 2 nm) on a spherical carbon shell containing Ni particles, in which electrons transfer from the anchored Ru clusters in the carbon layer to the core Ni particles. The formation of electron-deficient Ru sites facilitated the modulation of hydrogen adsorption capability and thus promoted the HER process with an ultra-low overpotential of 309 mV at 1000 mA, a Tafel slope of 27 mV·dec^{-1}, and a TOF of 30.5 H_2 at -0.1 V·s^{-1}. Liu et al. [71] fabricated a rich array of protrusion Cu@NiRu core-shell nanotubes by the wet chemistry method shown in Figure 4e. The unique one-dimensional hollow structure can effectively prevent nanoparticle aggregation, thus stabilizing the RuNi alloy shell layer (Figure 4f) and obtaining catalysts with the best performance (Cu@$Ni_{19}Ru_{81}$ NTs/C). Ni/Cu alloy attenuated the binding of H_2 on the Ru sites, which enabled the dynamic electron exchange between Ru and Ni/Cu and optimized the electronic structure at the surface by transferring electrons from Ni to Ru. The Cu@$Ni_{19}Ru_{81}$ NTs/C had the optimal ΔG_H* (Figure 4g), realizing the enhancement of HER performance with an overpotential of only 22 mV at 10 mA·cm^{-2}, a Tafel slope of about 29.6 mV·dec^{-1} (Figure 4h), and good stability after 5000 cycles of voltammetry (Figure 4i).

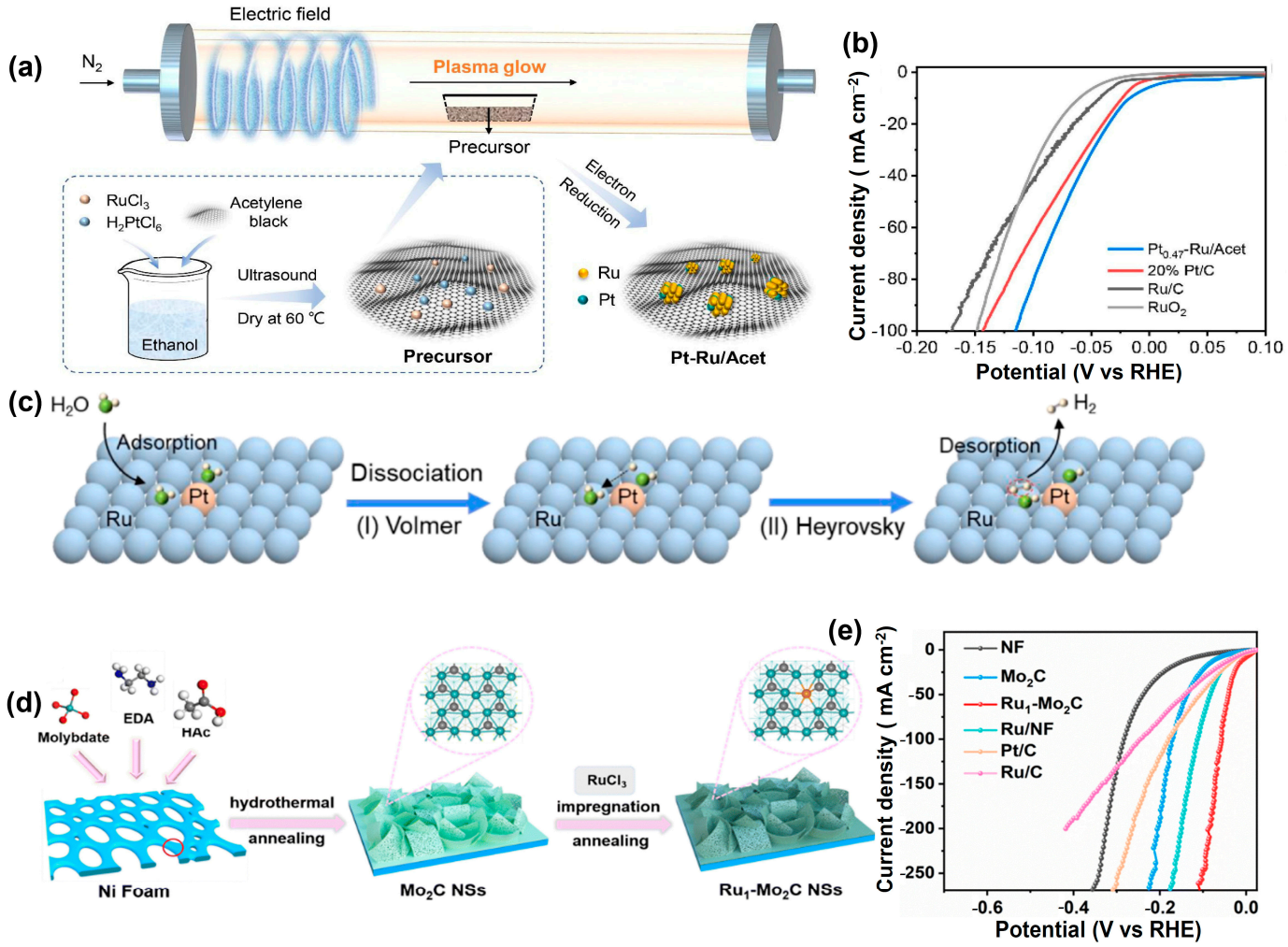


Figure 3. (**a**) A synthesis strategy diagram of $Pt_{0.47}$-Ru/Acet. (**b**) LSV polarization curves (IR corrected) of Ni foam (NF), Acet, Ru/Acet, $Pt_{0.47}$-Ru/Acet, Pt/C, 5 wt% Ru/C, and RuO_2 at a scan rate of 10 $mV \cdot s^{-1}$. (**c**) A schematic diagram of the alkaline HER mechanism on Pt-Ru/Acet. (**d**) The synthesis and characterization of Ru_1-Mo_2C NSs. (**e**) HER polarization curves of NF, Ru_1-Mo_2C NSs, Mo_2C NSs, Ru/NF, and Pt/C electrocatalysts in 1 M KOH electrolyte. Reproduced with permission from the authors of [53,60]. Copyright © 2022 Elsevier B.V. and 2024 Royal Society of Chemistry.

4.3. Ruthenium-Based Compounds

In addition to metallic Ru-based catalysts, Ru-based compounds such as ruthenium oxide (RuO_2), ruthenium complex hydroxides, ruthenium phosphide, ruthenium sulfide, and ruthenium selenide can enhance the electronic structure of metallic Ru and have higher stability than metallic catalysts, thus providing excellent electrocatalytic performance.

The formation of a metal/metal oxide interface facilitates the efficient adsorption of H* at the interface and releases H_2 from the catalyst surface with ΔG_H* approaching zero, which is a reliable technique to boost the effectiveness of HER in non-acidic environments [72,73]. Dang et al. [74] employed a combination of heating and in situ electrochemical reduction in an anoxic environment to achieve a partial reduction in RuO_2. The Ru/RuO_2 interface exhibited robust active sites for water adsorption and dissociation, coupled with an optimal H and OH binding energy, thus exhibiting good alkaline HER performance. It also had adequate −H and −OH stabilization energies and thus exhibited superior activity with an overpotential of 17 mV to reach a current density of 10 $mA \cdot cm^{-2}$ and a Tafel slope value of 35 $mV \cdot dec^{-1}$. Li et al. [75] assembled sub-nanometer-sized RuO_2 shells with oxygen-rich vacancies onto linked Ru clusters/carbon hybridized microchips (Ru@V-RuO_2/C HMS), as shown in Figure 5a. The shells of the oxygen-rich exoskeleton

can synergistically change the electronic structure of the interface to bring the adsorption of OH intermediates closer to the desired level, which accelerates the H generation kinetics and enhances the alkaline HER performance with an ultra-low overpotential of 6 mV at 10 mA·cm^{-2} (Figure 5b) and a decay ratio of the potential of only 0.93% h^{-1}. Chen et al. [76] reported a novel carbon-loaded Ru/RuO_2 nano boomerang (Ru/RuO_2 NB/C), in which Ru/RuO_2 NB exposed with a new Janus nanostructure with two arms of Ru and RuO_2 active sites independent of each other without inhibiting their activities. The Ru/RuO_2 NB had proper H* and OH* binding energies and showed 5.3 times higher HER metal mass activity than that of commercial RuO_2/C.

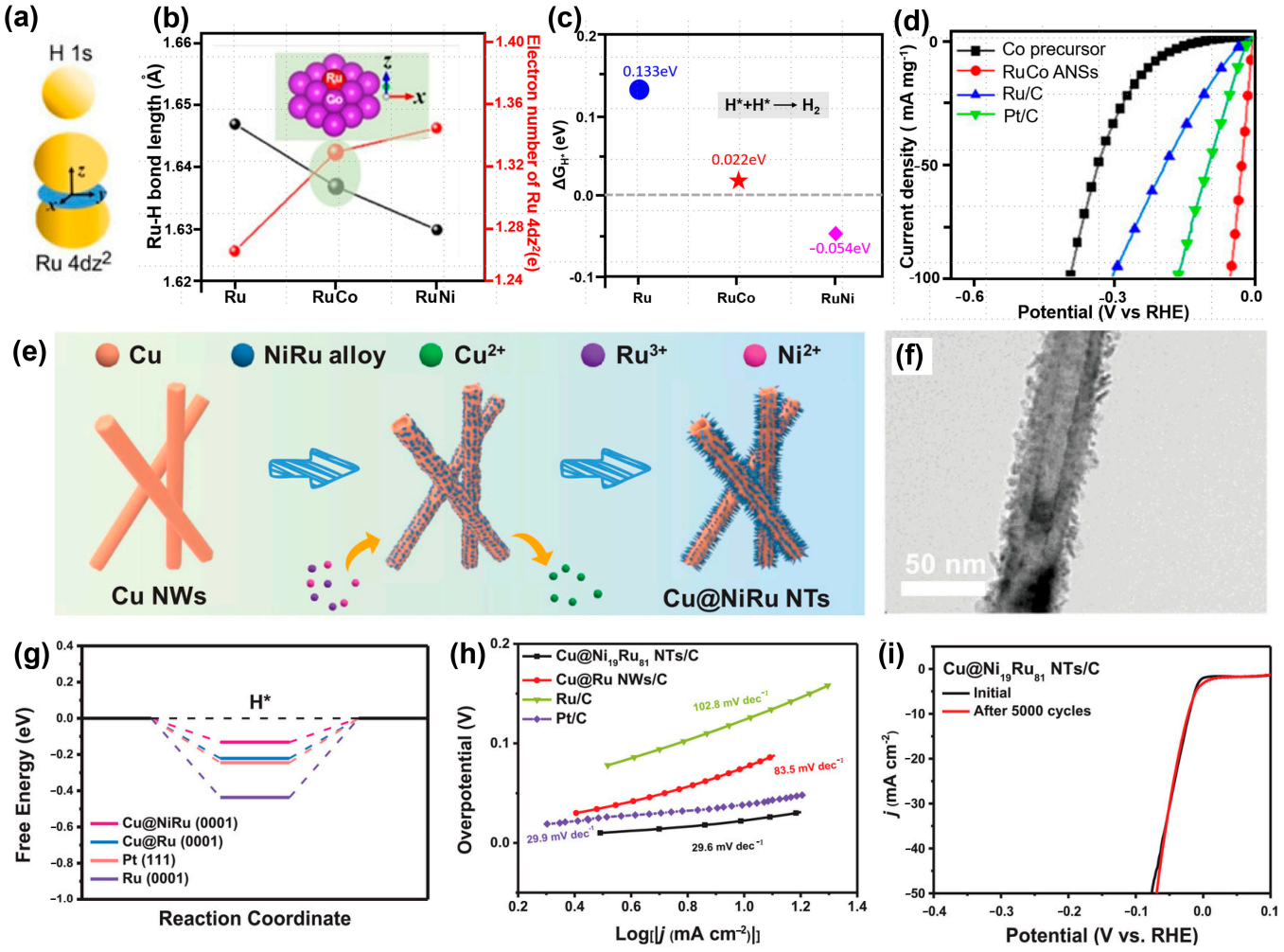


Figure 4. (**a**) Schematic diagram of orbital coupling between Ru 4d$_z^2$ and H 1s. (**b**) The Ru-H bond lengths and electron numbers of Ru 4d$_z^2$ in Ru, RuCo, and RuNi models. The inset shows the plane-symmetric and Z-direction asymmetric coordination structures of the RuCo model. (**c**) The H* Gibbs free energy for Ru, RuCo, and RuNi models. (**d**) The polarization curves of Co precursor, RuCo ANSs, Ru/C, and Pt/C. (**e**) Synthetic strategy of Cu@NiRu NTs. (**f**) TEM. (**g**) Free energy diagram for H adsorption. (**h**) Tafel slopes of Cu@$Ni_{19}Ru_{81}$ NTs/C, Cu@Ru NWs/C, Ru/C, and Pt/C. (**i**) Polarization curves of Cu@$Ni_{19}Ru_{81}$ NTs/C before and after 5000 CV cycles. Reproduced with permission from the authors of [64,71]. Copyright © 2021 Wiley-VCH GmbH and 2022 Wiley-VCH GmbH.

In nickel-based hydroxides, the collaborative impact of Ni(OH)$_2$ and Ru regulates the electronic structure of the catalyst, optimizes the energy barriers, and accelerates the charge transfer rate of the catalytic reaction. The special porous structure of nickel foam substrate [77] can enhance the exposure of active sites and the stability of the material. Lin et al. [78] synthesized Ru/Ni(OH)$_2$/NF by a high-temperature solid-phase method,

which had an overpotential of 42 mV at -10 mA·cm^{-2}. $Fe(OH)_5$ significantly improved the alkaline HER performance of Ru NPs by modulating the electronic structure and establishing a connection between Ru and $Fe(OH)_5$. Liu et al. [79] prepared RuFe@NF via a one-pot impregnation approach at room temperature, as shown in Figure 5c–f. The performance of RuFe@NF as an integral water separation of the cathode and anode in a bipolar system has been investigated (Figure 5g). As illustrated in Figure 5h,i, this system exhibited the best performance and maintained good stability after 680 h of continuous operation. In addition, RuFe@NF can reach a current density of -10 mA·cm^{-2} at 28 mV with a Tafel slope of 63.39 mV·dec^{-1}. Mo et al. [80] used the acid etch-assisted electrodeposition method to prepare $Fe(OH)_5$ -Ru/$Ni(OH)_2$, which only required low overpotentials of 61, 127, and 170 mV to achieve current densities of -100, -500, and -800 mA·cm^{-2}.

A Ru-H bond energy that is too weak leads to ineffective proton adsorption in the HER process, while a Ru-H bond that is too strong poisons Ru sites and prevents the formation of H_2 [26]. The strength of the Ru-H bond can be tuned by designing of ruthenium phosphide or semiconductor sulfide [81] because S and P atoms can extract electrons from Ru to modify the 4d electronic orbital and the H binding energy of Ru. The interaction of phosphides with interfacial electrons leads to the charge redistribution of RuP, which results in the shifting of the d-band center upward to the Fermi level of RuP to have an optimal hydrogen binding strength. Li et al. [82] obtained RuP/Ru@CNS by a high-temperature solid-phase method shown in Figure 6a. As influenced by the energy barrier of the hydrogen spillover at the RuP/Ru interface (Figure 6b), the spillover energy barrier of H^* from Ru atoms in hetero-Ru (site 2) to the ones in hetero-RuP (site 3) is only 0.11 eV, and thus the H^* produced on hetero-Ru can be transferred easily to hetero-RuP and desorbed to generate H_2, which improved the HER kinetics. RuP/Ru@CNS required overpotentials of only 15, 50, and 73 mV at -10, -50, and -100 mA·cm^{-2} (Figure 6c) and a Tafel slope of 32 mV·dec^{-1} (Figure 6d). Li et al. [83] obtained RuP/NP-C with the full exposure of active sites and a rapid mass/charge transfer, which exhibited the respectable HER performance of having an overpotential of 40 mV at -10 mA·cm^{-2} and a Tafel slope of 49.0 mV·dec^{-1}. At a constant current density of 10 mA·cm^{-2}, RuP/NP-C can be largely maintained with only a slight decay over 18 h.

Zhou et al. [84] used hydrothermal phosphorylation to synthesize Ru/P-TiO_2, which formed a reversible hydrogen spillover mode by the introduction of P to reduce the Tafel slope and accelerate the hydrogen production from the HER. The overpotential was only 27 mV at -10 mA·cm^{-2}, the Tafel slope was 28.3 mV·dec^{-1}, and the overpotential increased by only 6 mV after 2000 cycles. Ru atoms within the configuration of Ru_2P were displaced by M = Co, Ni, or Mo to fabricate $M_xRu_{2-x}P$ nanocrystals. The existence of Co or Ni in the tetrahedral positions brought forth a charge reallocation of Ru, and metals with phosphide structures showed positional preferences, where Co and Ni were situated in the tetrahedral positions of the CoRuP and NiRuP (Ru_2P-type), and Ru occupied the tetragonal cone positions. The positional preferences of Co and Ni lead to a beneficial alteration of the electronic structure of Ru that shifts the center of the d-band upward. El-Refaei et al. [85] synthesized a catalyst of $M_{2-x}Ru_xP$ nanocrystalline catalysts with the identical orthorhombic crystal structure as Ru_2P by pyrolysis, driving current densities of -10 and -100 mA·cm^{-2}, which required overpotentials of 12.9 and 43.5 mV for CoRuP, 16.0 and 60.8 mV for NiRuP23.7, and 77.6 mV for MoRuP.

Transition metal disulfide compounds (TMDs) have become a trending research theme in the area of electrocatalysis, especially in the HER due to their remarkable catalytic performance, chemical stability, and economic efficiency. In addition to their metal active sites, the abundant sulfur sites and selenium sites in these materials can also serve as active centers that electronically adsorb and contribute to the acceleration of the overall kinetics [86]. Doping of Ru induced a partial phase transition of MoS_2 from triangular (2 H) to octahedral (1 T) phases with the simultaneous generation of sulfur vacancies [87]. The induced phase transition not only activated the non-reactive base surface of MoS_2 but also lowered the energy barriers for the adsorption/desorption of H* intermediates. When

OH^* migrated from Ru to MoS_2, the poisoning of Ru sites can be alleviated [88]. Apart from the structural enhancements, the built-in synergistic outcomes connected with the electronic configuration alteration and defect engineering, along with increased Ru atom utilization, significantly contributed to the enhanced electrochemical HER performance. Zhang et al. [89] obtained Ru-MoS_2/CNT by high-temperature solid-phase sintering, and the Ru-MoS_2/CNT displayed a small overpotential of 50 mV at -10 mA·cm^{-2} and a low Tafel slope of 62 mV·dec^{-1}. Islam et al. [90] used a top-down method for the in situ preparation of Ru@MoS_2/GO, which had an overpotential of 60 mV at -10 mA·cm^{-2}, a Tafel slope of 38 mV·dec^{-1}, and a remarkable durability during 10 h of continuous operation at 100 mV potential. Li et al. [91] prepared Ru monolayer islands doped with MoS_2 nanosheets (Ru MIs-MoS_2) in a rotating packed bed (RPB) reactor, which had a low overpotential of 17 mV at 10 mA·cm^{-2} under alkaline conditions.

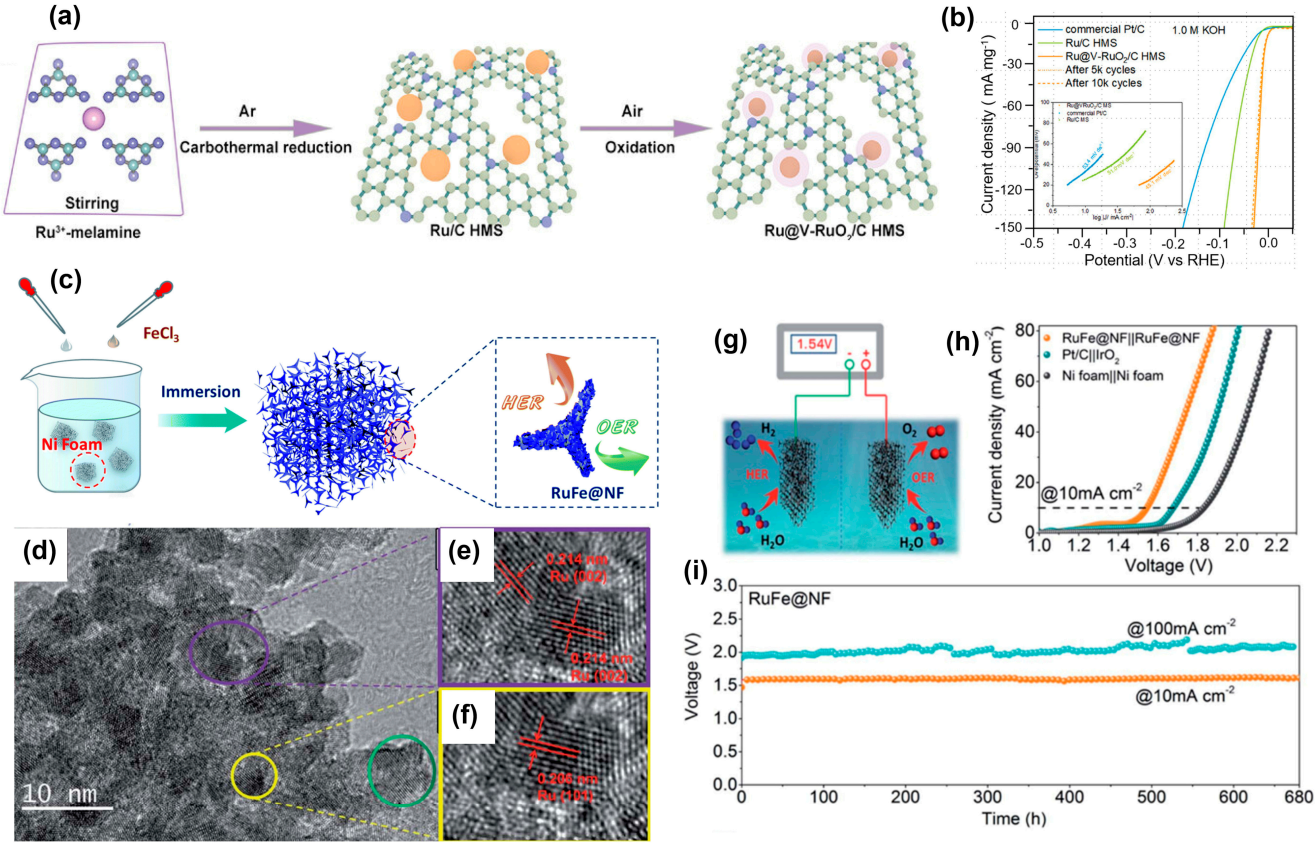


Figure 5. (**a**) Schematic illustration to prepare Ru@V-RuO_2/C HMS. (**b**) HER polarization curves of Pt/C, Ru/C HMS, and Ru@V-RuO_2/C HMS, and their subsequent curves during different cycles in 1.0 M KOH. The insets in (**b**) show the corresponding Tafel slope plots. (**c**) The synthetic process of RuFe@NF and its TEM images (**d**–**f**). (**g**) A schematic diagram showing the two-electrode system for water splitting. (**h**) LSV curves of water splitting for the RuFe@NF, RuFe@NF||RuFe@NF, Pt/C||IrO_2, and Ni foam||Ni foam in 1 M KOH. (**i**) The stability of the RuFe@NF measured at a current response of 10 mA·cm^{-2} and 100 mA·cm^{-2}. Reproduced with permission from the authors of [75,79]. Copyright © 2023 Wiley-VCH GmbH and 2022 Royal Society of Chemistry.

Cai et al. [92] utilized a redox solid-phase interface reaction (SPIR) strategy to prepare highly defective MoS_2/RuO_2 composite flakes, as shown in Figure 6e, which had an overpotential of 12 mV at -10 mA·cm^{-2} (Figure 6f) and a Tafel slope of 50 mV·dec^{-1} (Figure 6g). Highly graphitized carbon nanotube carriers provided a fast electron transport pathway. Li et al. [86] synthesized $RuSe_2$ NPs, which uniformly dispersed across the CNTs. The pyrite-type $RuSe_2$ showed excellent alkaline HER performance with an overpotential of 29.5 mV at -10 mA·cm^{-2} and a Tafel slope of 39.2 mV·dec^{-1}. The anchoring of

$RuSe_2$ on the carbon nanotubes resulted in good stability, and the current density remained undiminished after performing 2000 CV cycles. Zhao et al. [93] synthesized porous $RuSe_2$ with different crystallinity (amorphous, amorphous/crystalline, and crystalline) using a direct hydrothermal synthesis approach, followed by an annealing treatment. Results from comparative experiments illustrated that the porous structure of $RuSe_2$-400 °C and the interfacial spots between the crystalline and amorphous phases simultaneously possessed abundant unsaturated coordination, which ensured the superior conductance of the material. The binding energy of the transitional states was optimized by modifying the electronic structure of $RuSe_2$-400 °C. $RuSe_2$-400 °C with a crystalline/amorphous structure exhibited better activity compared to its non-crystalline and crystalline forms, showing an overpotential of 27 mV and a Tafel slope of 39.2 $mV \cdot dec^{-1}$ at 10 $mA \cdot cm^{-2}$. Cu doping and the combined impact of heterogeneous interfacial structure not only optimized the electronic structure of the heterogeneous interface and the d-band centers but also lowered the energy threshold by boosting the adsorption capability for H_2O. Wang et al. [33] designed Cu-doped Ru/$RuSe_2$ heterogeneous NSs, which not only possessed the overpotential of 23 mV, Tafel slope of 58.5 $mV \cdot dec^{-1}$ at −10 $mA \cdot cm^{-2}$, and TOF of 0.88 s^{-1} at 100 mV but also showed maintained activity after 5000 cycles of potential sweeps. Table 1 summarizes the alkaline HER performance of partial Ru-based catalysts mentioned in this review.

Table 1. Alkaline HER performances of selected ruthenium-based catalysts.

Catalyst	Electrolyte	Tafel Plot ($mV \cdot dec^{-1}$)	Overpotential (mV) @10 $mA \cdot cm^{-2}$	Reference
CP100C Ru	1 M KOH	20.0	4.7	[43]
Ru/C-600	1 M KOH	33.7	30.0	[44]
Ru NCs/NC	1 M KOH	64.7	14.0	[31]
Ru NCs/BNG	1 M KOH	28.9	14.0	[38]
P-Ru-3/C	1 M KOH	105.0	31.0	[45]
Ru@N-P-C-800	1 M KOH	115.0	45.0	[46]
Ru-S/N-C	1 M KOH	36.0	10.0	[39]
RuCo-CAT/CC	1 M KOH	32.1	38.0	[49]
CoRu-BPDC	1 M KOH	73.2	37.0	[51]
$Pt_{0.47}$-Ru/Acet	1 M KOH	66.0	17.0	[53]
PtRu/mCNTs	1 M KOH	33.5	15.0	[55]
PtRu/CC 1500	1 M KOH	25.0	19.0	[56]
RuMo/NC	1 M KOH	52.8	24.0	[54]
P,Mo-Ru@PC	1 M KOH	21.7	21.0	[57]
Ru_1-Mo_2C NPs	1 M KOH	38.5	10.8	[60]
Mo-Ru NSAs	1 M KOH	16.1	16.0	[62]
RuCo ANSs	1 M KOH	20.6	10.0	[64]
Ru-Co@Ti_2AlC	1 M KOH	105.0	25.0	[63]
a-Ru@Co-DHC	1 M KOH	62.0	40.0	[65]
M-Co NPs@Ru SAs/NC	1 M KOH	55.0	34.0	[66]
Ru-Ni	1 M KOH	25.9	23.0	[69]
Ru/Ni@C	1 M KOH	27.0	15.0	[70]
Cu@$Ni_{19}Ru_{81}$ NTs/C	1 M KOH	29.6	22.0	[71]
RuO_2-300Ar	1 M KOH	35.0	17.0	[74]
Ru@V-RuO_2/C HMS	1 M KOH	45.1	6.0	[75]
Ru/RuO_2 NB/C	1 M KOH	45.1	54.0	[76]
RuFe@NF	1 M KOH	63.4	28.0	[79]
RuP/Ru@CNS	1 M KOH	32.0	15.0	[82]
RuP/NP-C	1 M KOH	49.0	40.0	[83]
Ru/P-TiO_2	1 M KOH	28.3	27.0	[84]
CoRuP	1 M KOH	30.0	12.9	[85]
Ru-MoS_2/CNT	1 M KOH	62.0	50.0	[89]
Ru@MoS_2/GO	1 M KOH	38.0	60.0	[90]
Ru MIs-MoS_2	1 M KOH	63.0	17.0	[91]
MiSC-1	1 M KOH	50.0	12.0	[92]
$RuSe_2$	1 M KOH	39.2	29.5	[86]
$RuSe_2$-400 C	1 M KOH	39.2	27.0	[93]
Cu-doped Ru/$RuSe_2$	1 M KOH	58.5	23.0	[33]

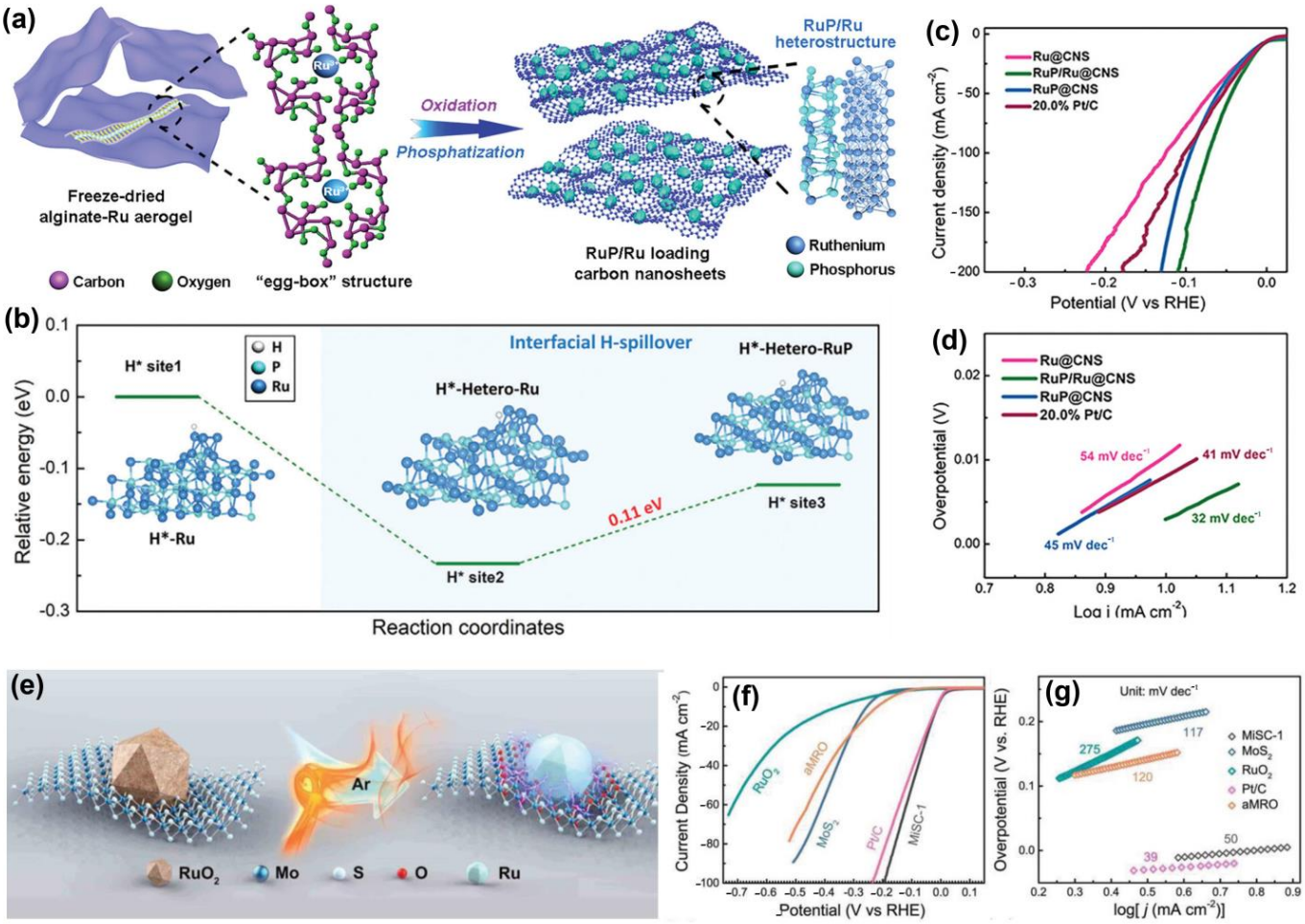


Figure 6. (**a**) The synthesis of RuP/Ru@CNS. (**b**) The calculated energy barrier for hydrogen spillover between Ru atoms at the RuP/Ru interface. (**c**) IR-corrected HER LSV curves and (**d**) Tafel plots of Ru@CNS, RuP/Ru@CNS, RuP@CNS, 20.0% Pt/C in alkaline media. (**e**) The fabrication process of MiSC-1. (**f**) HER polarization curves and (**g**) Tafel plots of MiSC-1, Pt/C, MoS_2, RuO_2, and aMRO. Reproduced with permission from the authors of [82,92]. Copyright © 2024 Wiley-VCH GmbH and 2021 Wiley-VCH GmbH.

5. Conclusions and Future Outlooks

In this review, we first discuss the principles, performance-influencing factors, and regulation strategies for the performance improvement of the alkaline HER in water electrolysis. Then the research progress of ruthenium-based catalysts for the alkaline HER is summarized with selected examples. The electronic structures of various ruthenium nanoparticles, ruthenium-M heterogeneous catalysts, and ruthenium-based compounds are regulated by modulating the components and ligands of Ru atoms, aiming to achieve low water dissociation energies and optimal binding energies for hydrogen (H) and hydroxyl (-OH) groups, thereby enhancing the alkaline HER catalytic performance. Fruitful results have been achieved, while the following problems, challenges, and future development directions should be paid attention to:

(1) The development of simple and economical synthesis methods for Ru-based catalysts. At this stage, the assessment of Ru-based catalysts remains in the laboratory stage. Most catalysts are prepared by complicated and cumbersome methods with high costs. In particular, the high-temperature pyrolysis of precursors has been commonly employed to produce Ru-based catalysts for hydrogen generation. At high temperatures, metallic Ru is highly susceptible to aggregation despite the use of a carrier with high conductivity and a large specific surface area. Accordingly, investigating

low-temperature and scalable synthesis techniques, like electrochemical replacement reactions and wet chemical reduction, could help avoid the aggregation of Ru, thus exposing more catalytic sites and improving catalytic efficiency as well as lowering the cost, making such techniques more likely to enter into practical or industrial production and applications [94,95].

(2) The standardization of electrochemical measurements and analysis. Standardized electrochemical measurements and analysis must be performed to accurately and fairly evaluate the performance of catalysts in different laboratories, including rational and accurate three-electrode configurations, the geometric area of electrodes, mass loading, normalized activity, and TOF calculation methods. The utilization of a rotating disk electrode (RDE) as the working electrode facilitates more precise outcomes for Ru-based powder catalysts. Furthermore, to obtain experimental results with good application prospects, the experimental scale should be expanded to narrow the gap between experimental research and industrial applications. It is recommended to conduct electrochemical measurements under actual equipment operation, such as a high current density at the ampere level [12,18,96].

(3) The combination of in situ/operando characterizations with theoretical calculations to elucidate the structure–performance relationships. In the alkaline HER, the intrinsic catalytic performance of catalysts is influenced by ΔG_{H^*}, the adsorption and dissociation of H_2O, and the strength of -OH adsorption, and the related reaction mechanisms of different systems remain unclear. Therefore, it is necessary to characterize the reaction process in situ/operando to capture the information of interfacial water and intermediate species such as -H and -OH and, at the same time, combine this information with detailed and advanced theoretical calculations to deduce the reaction pathways and mechanisms, to reveal the structure–performance relationship and to provide guidance for the design of advanced catalysts. The advancement of material science, in situ/operando characterization methods, and theoretical simulations will facilitate a significant expansion in the production of hydrogen from alkaline water electrolysis. It is anticipated that the metal Ru, which has the potential to serve as an effective alternative to Pt, will be widely adopted in the large-scale design of alkaline HER catalysts [97–99].

Author Contributions: Conceptualization: X.-M.L.; Writing—original draft preparation: X.-M.L. and B.-L.L.; Writing—reviewing and editing: X.C., B.-T.N., Y.-T.L., X.-M.L. and Y.-X.C.; supervision, X.-M.L. and Y.-X.C.; project administration, X.-M.L.; funding acquisition, X.-M.L., Y.-X.C. and X.C. All authors have read and agreed to the published version of the manuscript.

Funding: This research was funded by the National Natural Science Foundation of China (22272069 and 22472074), the Natural Science Foundation of Fujian Province (2021J01988 and 2023H0046), the XMIREM autonomously deployment project (2023CX10 and 2023GG01), and Postdoctoral Fellowship Program of CPSF (GZC20240897).

Data Availability Statement: Not applicable.

Conflicts of Interest: The authors declare no conflicts of interest.

References

1. Chesshire, J. Energy crisis. *Nature* **1977**, *269*, 269. [CrossRef]
2. Guerra, O.J.; Eichman, J.; Denholm, P. Optimal energy storage portfolio for high and ultrahigh carbon-free and renewable power systems. *Energy Environ. Sci.* **2021**, *14*, 5132–5146. [CrossRef]
3. Mackey, B.; Lindenmayer, D. Fossil fuels' future. *Science* **2014**, *345*, 739–740. [CrossRef]
4. Gibson, L.; Wilman, E.N.; Laurance, W.F. How green is "green" energy? *Trends Ecol. Evol.* **2017**, *32*, 922–935. [CrossRef]
5. Xu, X.M.; Zhong, Y.J.; Wajrak, M.; Bhatelia, T.; Jiang, S.P.; Shao, Z.P. Grain boundary engineering: An emerging pathway toward efficient electrocatalysis. *InfoMat* **2024**, *6*, e12608. [CrossRef]
6. Sun, H.N.; Kim, H.; Song, S.Z.; Jung, W. Copper foam-derived electrodes as efficient electrocatalysts for conventional and hybrid water electrolysis. *Mater. Rep. Energy* **2022**, *2*, 100092. [CrossRef]

7. Stamenkovic, V.R.; Strmcnik, D.; Lopes, P.P.; Markovic, N.M. Energy and fuels from electrochemical interfaces. *Nat. Mater.* **2017**, *16*, 57–69. [CrossRef]
8. Hota, P.; Das, A.; Maiti, D.K. A short review on generation of green fuel hydrogen through water splitting. *Int. J. Hydrogen Energy* **2023**, *48*, 523–541. [CrossRef]
9. Yan, X.Y.; Biemolt, J.; Zhao, K.; Zhao, Y.; Cao, X.J.; Yang, Y.; Wu, X.Y.; Rothenberg, G.; Yan, N. A membrane-free flow electrolyzer operating at high current density using earth-abundant catalysts for water splitting. *Nat. Commun.* **2021**, *12*, 4143. [CrossRef]
10. He, Q.; Zhou, Y.Z.; Shou, H.W.; Wang, X.Y.; Zhang, P.J.; Xu, W.J.; Qiao, S.C.; Wu, C.Q.; Liu, H.J.; Liu, D.B.; et al. Synergic reaction kinetics over adjacent ruthenium sites for superb hydrogen generation in alkaline media. *Adv. Mater.* **2022**, *34*, 2110604. [CrossRef]
11. Abdelghafar, F.; Xu, X.M.; Jiang, S.P.; Shao, Z.P. Designing single-atom catalysts toward improved alkaline hydrogen evolution reaction. *Mater. Rep. Energy* **2022**, *2*, 100144. [CrossRef]
12. Luo, W.J.; Wang, Y.J.; Cheng, C.W. Ru-based electrocatalysts for hydrogen evolution reaction: Recent research advances and perspectives. *Mater. Today Phys.* **2020**, *15*, 100274. [CrossRef]
13. Hu, S.L.; Li, W.X. Sabatier principle of metal-support interaction for design of ultrastable metal nano-catalysts. *Science* **2021**, *374*, 1360–1365. [CrossRef] [PubMed]
14. Guo, Y.; Tong, X.L.; Yang, N.J. Design and performance of Rh nanocatalysts for boosted H_2 generation in alkaline media. *Acc. Mater. Res.* **2024**, *5*, 89–102. [CrossRef]
15. Zheng, Y.; Jiao, Y.; Zhu, Y.H.; Li, L.H.; Han, Y.; Chen, Y.; Jaroniec, M.; Qiao, S.Z. High electrocatalytic hydrogen evolution activity of an anomalous ruthenium catalyst. *J. Am. Chem. Soc.* **2016**, *138*, 16174–16181. [CrossRef]
16. Pan, S.Y.; Li, C.; Xiong, T.T.; Xie, Y.H.; Luo, F.; Yang, Z.H. Hydrogen spillover in MoO_xRh hierarchical nanosheets boosts alkaline HER catalytic activity. *Appl. Catal. B Environ.* **2024**, *341*, 123275. [CrossRef]
17. Wu, H.; Huang, Q.X.; Shi, Y.Y.; Chang, J.W.; Lu, S.Y. Electrocatalytic water splitting: Mechanism and electrocatalyst design. *Nano Res.* **2023**, *16*, 9142–9157. [CrossRef]
18. Guo, F.; Macdonald, T.J.; Sobrido, A.J.; Liu, L.X.; Feng, J.R.; He, G.J. Recent advances in ultralow-Pt-loading electrocatalysts for the efficient hydrogen evolution. *Adv. Sci.* **2023**, *10*, 2301098. [CrossRef]
19. López, M.; Exner, K.S.; Viñes, F.; Illas, F. Theoretical study of the mechanism of the hydrogen evolution reaction on the V_2C MXene: Thermodynamic and kinetic aspects. *J. Catal.* **2023**, *421*, 252–263. [CrossRef]
20. Chen, D.C.; Chen, Z.W.; Zhang, X.X.; Lu, Z.L.; Xiao, S.; Xiao, B.B.; Singh, V.C. Exploring single atom catalysts of transition-metal doped phosphorus carbide monolayer for HER: A first-principles study. *J. Energy Chem.* **2021**, *52*, 155–162. [CrossRef]
21. Wei, J.M.; Zhou, M.; Long, A.C.; Xue, Y.M.; Liao, H.B.; Wei, C.; Xu, J.Z. Heterostructured electrocatalysts for hydrogen evolution reaction under alkaline conditions. *Nano Micro Lett.* **2018**, *10*, 75. [CrossRef] [PubMed]
22. Zhu, J.; Hu, L.S.; Zhao, P.X.; Lee, L.Y.S.; Wong, K.Y. Recent advances in electrocatalytic hydrogen evolution using nanoparticles. *Chem. Rev.* **2020**, *120*, 851–918. [CrossRef] [PubMed]
23. Yang, Y.J.; Yu, Y.H.; Li, J.; Chen, Q.R.; Du, Y.L.; Rao, P.; Li, R.S.; Jia, C.M.; Kang, Z.Y.; Deng, P.L.; et al. Engineering ruthenium-based electrocatalysts for effective hydrogen evolution reaction. *Nano Micro Lett.* **2021**, *13*, 160. [CrossRef] [PubMed]
24. Wang, P.F.; Zhan, S.H.; Xia, Y.G.; Ma, S.L.; Zhou, Q.X.; Li, Y. The fundamental role and mechanism of reduced graphene oxide in rGO/Pt-TiO_2 nanocomposite for high-performance photocatalytic water splitting. *Appl. Catal. B Environ.* **2017**, *207*, 335–346. [CrossRef]
25. Hu, Q.; Gao, K.R.; Wang, X.D.; Zheng, H.J.; Cao, J.Y.; Mi, L.R.; Huo, Q.H.; Yang, H.P.; Liu, J.H.; He, C.X. Subnanometric Ru clusters with upshifted D band center improve performance for alkaline hydrogen evolution reaction. *Nat. Commun.* **2022**, *13*, 3958. [CrossRef]
26. Ma, X.F.; Xiao, H.; Gao, Y.; Zhao, M.; Zhang, L.; Zhang, J.; Jia, J.F.; Wu, H.S. Enhancement of pore confinement caused by the mosaic structure on Ru nanoparticles for pH-universal hydrogen evolution reaction. *J. Mater. Chem. A* **2023**, *11*, 3524–3534. [CrossRef]
27. Li, L.L.; Tian, F.Y.; Qiu, L.Y.; Wu, F.Y.; Yang, W.W.; Yu, Y.S. Recent progress on ruthenium-based electrocatalysts towards the hydrogen evolution reaction. *Catalysts* **2023**, *13*, 1497. [CrossRef]
28. Zhou, B.H.; Gao, R.J.; Zou, J.J.; Yang, H.M. Surface design strategy of catalysts for water electrolysis. *Small* **2022**, *18*, 2202336. [CrossRef]
29. Luo, M.; Cai, J.Y.; Zou, J.S.; Jiang, Z.; Wang, G.M.; Kang, X.W. Promoted alkaline hydrogen evolution by an N-doped Pt–Ru single atom alloy. *J. Mater. Chem. A* **2021**, *9*, 14941–14947. [CrossRef]
30. Alsabban, M.M.; Eswaran, M.K.; Peramaiah, K.; Wahyudi, W.; Yang, X.L.; Ramalingam, V.; Hedhili, M.N.; Miao, X.H.; Schwingenschlögl, U.; Li, L.J.; et al. Unusual activity of rationally designed cobalt phosphide/oxide heterostructure composite for hydrogen production in alkaline medium. *ACS Nano* **2022**, *16*, 3906–3916. [CrossRef]
31. Huang, X.X.; Lu, R.H.; Cen, Y.P.; Wang, D.C.; Jin, S.; Chen, W.X.; Geoffrey, I.; Waterhouse, N.; Wang, Z.Y.; Tian, S.B.; et al. Micropore-confined Ru nanoclusters catalyst for efficient pH-universal hydrogen evolution reaction. *Nano Res.* **2023**, *16*, 9073–9080. [CrossRef]
32. van Deelen, T.W.; Hernández Mejía, C.; de Jong, K.P. Control of metal-support interactions in heterogeneous catalysts to enhance activity and selectivity. *Nat. Catal.* **2019**, *2*, 955–970. [CrossRef]

33. Wang, K.; Zhou, J.H.; Sun, M.Z.; Lin, F.X.; Huang, B.L.; Lv, F.; Zeng, L.Y.; Zhang, Q.H.; Gu, L.; Luo, M.C.; et al. Cu-doped heterointerfaced Ru/$RuSe_2$ nanosheets with optimized H and H_2O adsorption boost hydrogen evolution catalysis. *Adv. Mater.* **2023**, *35*, 2300980. [CrossRef]
34. Wang, Y.; Zheng, P.; Li, M.X.; Li, Y.R.; Zhang, X.; Chen, J.; Fang, X.; Liu, Y.J.; Yuan, X.L.; Dai, X.P.; et al. Interfacial synergy between dispersed Ru sub-nanoclusters and porous NiFe layered double hydroxide on accelerated overall water splitting by intermediate modulation. *Nanoscale* **2020**, *12*, 9669–9679. [CrossRef] [PubMed]
35. Wang, D.; Liu, W.; Wang, H.N.; Lu, S.F.; Li, Y.Q.; Lu, L.; Yu, L.F.; Xiang, Y. Insight into in situ grown Ru-based integrated electrodes for hydrogen evolution reaction: Boosted mass transfer efficiency and promoted intrinsic activity. *Chem. Eng. J.* **2024**, *485*, 149807. [CrossRef]
36. Vayssilov, G.N.; Lykhach, Y.; Migani, A.; Staudt, T.; Petrova, G.P.; Tsud, N.; Skála, T.; Bruix, A.; Illas, F.; Prince, K.C.; et al. Support nanostructure boosts oxygen transfer to catalytically active platinum nanoparticles. *Nat. Mater.* **2011**, *10*, 310–315. [CrossRef]
37. Sarawutanukul, S.; Phattharasupakun, N.; Sawangphruk, M. 3D CVD graphene oxide-coated Ni foam as carbo-and electrocatalyst towards hydrogen evolution reaction in acidic solution: In situ electrochemical gas chromatograph. *Carbon* **2019**, *151*, 109–119. [CrossRef]
38. Ye, S.H.; Luo, F.Y.; Xu, T.T.; Zhang, P.Y.; Shi, H.D.; Qin, S.Q.; Wu, J.P.; He, C.X.; Ouyang, X.P.; Zhang, Q.L.; et al. Boosting the alkaline hydrogen evolution of Ru nanoclusters anchored on B/N–doped graphene by accelerating water dissociation. *Nano Energy* **2020**, *68*, 104301. [CrossRef]
39. Li, C.F.; Zhao, J.W.; Xie, L.J.; Wang, Y.; Tang, H.B.; Zheng, L.R.; Li, G.R. N coupling with S-coordinated Ru nanoclusters for highly efficient hydrogen evolution in alkaline media. *J. Mater. Chem. A* **2021**, *9*, 12659–12669. [CrossRef]
40. Liao, P.S.; Kang, J.W.; Zhong, Y.C.; Xiang, R.N.; Wang, S.H.; Li, S.S.; Liu, X.L.; Li, G.Q. Recent advances of two-dimensional metal-organic frameworks in alkaline electrolysis water for hydrogen production. *Sci. China Chem.* **2023**, *66*, 1924–1939. [CrossRef]
41. Sun, Y.M.; Xue, Z.Q.; Liu, Q.L.; Jia, Y.L.; Li, Y.L.; Liu, K.; Lin, Y.Y.; Liu, M.; Li, G.Q.; Su, C.Y. Modulating electronic structure of metal-organic frameworks by introducing atomically dispersed Ru for efficient hydrogen evolution. *Nat. Commun.* **2021**, *12*, 1369. [CrossRef] [PubMed]
42. Zhao, X.J.; Pachfule, P.; Thomas, A. Covalent organic frameworks (COFs) for electrochemical applications. *Chem. Soc. Rev.* **2021**, *50*, 6871–6913. [CrossRef] [PubMed]
43. Thalluri, S.M.; Rodriguez-Pereira, J.; Zazpe, R.; Bawa, B.; Kolíbalová, E.; Jelinek, L.; Macak, J.M. Enhanced C-O functionality on carbon papers ensures lowering nucleation delay of ALD for Ru towards unprecedented alkaline HER activity. *Small* **2023**, *19*, 2300974. [CrossRef] [PubMed]
44. Li, Z.R.; An, L.L.; Song, M.; Zhao, T.H.; Zhang, J.J.; Zhang, C.; Li, Z.Z.; Wang, D.L. Tuning the hydrogen and hydroxyl adsorption on Ru nanoparticles for hydrogen electrode reactions via size controlling. *Chin. Chem. Lett.* **2023**, *34*, 107622. [CrossRef]
45. Zhao, Y.M.; Wang, X.W.; Cheng, G.Z.; Lou, W. Phosphorus-induced activation of ruthenium for boosting hydrogen oxidation and evolution electrocatalysis. *ACS Catal.* **2020**, *10*, 11751–11757. [CrossRef]
46. Ajmal, Z.; Arif, M.; Kumar, A.; Haq, M.U.; Du, Y.F.; Zhang, Y.C.; Abboud, M.; Qian, J.; Chen, Z.J.; Ni, B.J.; et al. Uniformaly distributed Ru nanoparticles over N, P co-doped porous carbon as a highly active trifunctional electrocatalyst. *Int. J. Hydrogen Energy* **2024**, *73*, 768–774. [CrossRef]
47. Sun, X.Z.; Gao, X.Y.; Chen, J.; Wang, X.; Chang, H.X.; Li, B.; Song, D.M.; Li, J.; Li, H.S.; Wang, N. Ultrasmall Ru nanoparticles highly dispersed on sulfur-doped graphene for HER with high electrocatalytic performance. *ACS Appl. Mater. Interfaces* **2020**, *12*, 48591–48597. [CrossRef]
48. Jin, S. How to effectively utilize MOFs for electrocatalysis. *ACS Energy Lett.* **2019**, *4*, 1443–1445. [CrossRef]
49. He, Y.Q.; Yan, F.; Zhang, X.; Zhu, C.L.; Zhao, Y.Y.; Geng, B.; Chou, S.L.; Xie, Y.; Chen, Y.J. Creating dual active sites in conductive metal-organic frameworks for efficient water splitting. *Adv. Energy Mater.* **2023**, *13*, 2204177. [CrossRef]
50. Zhu, Y.M.; Klingenhof, M.; Gao, C.L.; Koketsu, T.; Weiser, G.; Pi, Y.C.; Liu, S.H.; Sui, L.J.; Hou, J.R.; Li, J.L.; et al. Facilitating alkaline hydrogen evolution reaction on the hetero-interfaced Ru/RuO_2 through Pt single atoms doping. *Nat. Commun.* **2024**, *15*, 1447. [CrossRef]
51. Li, X.Y.; Luo, D.; Jiang, F.; Zhang, K.J.; Wang, S.X.; Li, S.F.; Zha, Q.Q.; Huang, Y.C.; Ni, Y.H. Electronic modulation of metal-organic frameworks caused by atomically dispersed Ru for efficient hydrogen evolution. *Small* **2023**, *19*, 2301850. [CrossRef] [PubMed]
52. Sun, X.H.; Hu, Y.P.; Fu, Y.Y.; Yang, J.; Song, D.M.; Li, B.; Xu, W.H.; Wang, N. Single Ru sites on covalent organic framework-coated carbon nanotubes for highly efficient electrocatalytic hydrogen evolution. *Small* **2024**, *20*, 2305978. [CrossRef] [PubMed]
53. Chen, Y.J.; Li, J.; Wang, N.; Zhou, Y.N.; Zheng, J.; Chu, W. Plasma-assisted highly dispersed Pt single atoms on Ru nanoclusters electrocatalyst for pH-universal hydrogen evolution. *Chem. Eng. J.* **2022**, *448*, 137611. [CrossRef]
54. Yang, H.B.; Ma, D.W.; Li, Y.; Zhao, Q.H.; Pan, F.; Zheng, S.S.; Lou, Z.R. Mo doped Ru-based cluster to promote alkaline hydrogen evolution with ultra-low Ru loading. *Chin. J. Struct. Chem.* **2023**, *42*, 100031. [CrossRef]
55. Pang, B.B.; Liu, X.K.; Liu, T.Y.; Chen, T.; Shen, X.Y.; Zhang, W.; Wang, S.C.; Liu, T.; Liu, D.; Ding, T.; et al. Laser-assisted high-performance PtRu alloy for pH-universal hydrogen evolution. *Energ. Environ. Sci.* **2022**, *15*, 102–108. [CrossRef]
56. Li, L.; Zhang, G.W.; Wang, B.; Yang, T.; Yang, S.C. Electrochemical formation of PtRu bimetallic nanoparticles for highly efficient and pH-universal hydrogen evolution reaction. *J. Mater. Chem. A* **2020**, *8*, 2090–2098. [CrossRef]
57. Li, C.; Jang, H.; Liu, S.G.; Kim, M.G.; Hou, L.Q.; Liu, X.E.; Cho, J. P and Mo dual doped Ru ultrasmall nanoclusters embedded in P-doped porous carbon toward efficient hydrogen evolution reaction. *Adv. Energy Mater.* **2022**, *12*, 2200029. [CrossRef]

58. Li, Y.F.; Li, L.S.; Xu, S.L.; Cui, K.; Wang, T.S.; Jiang, Z.; Li, J.Y. Hydrogen spillover mechanism at the metal–metal interface in electrocatalytic hydrogenation. *Angew. Chem.* **2024**, *136*, e202407810. [CrossRef]
59. Gao, X.R.; Xing, Z.; Wang, M.Y.; Nie, C.H.; Shang, Z.C.; Bai, Z.C.; Dou, S.X.; Wang, N.N. Comprehensive insights into solid-state electrolytes and electrode-electrolyte interfaces in all-solid-state sodium-ion batteries. *Energy Storage Mater.* **2023**, *60*, 102821. [CrossRef]
60. Chao, T.T.; Xie, W.B.; Hu, Y.M.; Zhao, T.H.; Chen, C.; Zhang, Z.D.; Yu, G.; Hong, X.; Jin, H.L.; Wang, D.S.; et al. Reversible hydrogen spillover at the atomic interface for efficient alkaline hydrogen evolution. *Energy Environ. Sci.* **2024**, *17*, 1397–1406. [CrossRef]
61. Okazoe, S.; Kusada, K.; Wu, D.S.; Yamamoto, T.; Toriyama, T.; Matsumura, S.; Kawaguchi, S.; Kubota, Y.; Kitagawa, H. Synthesis of Mo and Ru solid-solution alloy NPs and their hydrogen evolution reaction activity. *Chem. Commun.* **2020**, *56*, 14475–14478. [CrossRef] [PubMed]
62. Li, L.G.; Liu, S.H.; Zhan, C.H.; Wen, Y.; Sun, Z.F.; Han, J.J.; Chan, T.S.; Zhang, Q.B.; Hud, Z.W.; Huang, X.Q. Surface and lattice engineered ruthenium superstructures towards high-performance bifunctional hydrogen catalysis. *Energ. Environ. Sci.* **2023**, *16*, 157–166. [CrossRef]
63. Kutyła, D.; Pajić, M.N.K.; Lačnjevac, U.Č.; Marzec, M.M.; NElezović, N.R.; Żabiński, P. Ru–Co alloy coatings electrodeposited on a MAX phase substrate as efficient catalysts for the hydrogen evolution reaction. *Int. J. Hydrogen Energy* **2024**, *56*, 28–40. [CrossRef]
64. Cai, C.; Liu, K.; Zhu, Y.M.; Li, P.C.; Wang, Q.Y.; Liu, B.; Chen, S.Y.; Li, H.J.W.; Zhu, L.; Li, H.M.; et al. Optimizing hydrogen binding on Ru sites with RuCo alloy nanosheets for efficient alkaline hydrogen evolution. *Angew. Chem.* **2022**, *61*, e202113664. [CrossRef] [PubMed]
65. Yang, W.X.; Zhang, W.Y.; Liu, R.; Lv, F.; Chao, Y.G.; Wang, Z.C.; Guo, S.J. Amorphous Ru nanoclusters onto Co-doped 1D carbon nanocages enables efficient hydrogen evolution catalysis. *Chin. J. Catal.* **2022**, *43*, 110–115. [CrossRef]
66. Zhang, H.; Su, H.; Soldatov, M.A.; Li, Y.L.; Zhao, X.; Liu, M.H.; Zhou, W.L.; Zhang, X.X.; Sun, X.; Xu, Y.Z.; et al. Dynamic Co-Ru bond shrinkage at atomically dispersed Ru sites for alkaline hydrogen evolution reaction. *Small* **2021**, *17*, 2105231. [CrossRef]
67. Gao, X.R.; Zang, W.J.; Li, X.; Wang, Z.K.; Zheng, L.R.; Kou, Z.K. Achieving efficient alkaline hydrogen evolution reaction on long-range Ni sites in Ru clusters-immobilized Ni_3N array catalyst. *Chem. Eng. J.* **2023**, *451*, 138698. [CrossRef]
68. Ojha, K.; Saha, S.; Dagar, P.; Ganguli, A.K. Nanocatalysts for hydrogen evolution reactions. *Phys. Chem. Chem. Phys.* **2018**, *20*, 6777–6799. [CrossRef]
69. Chen, X.W.; Ye, L.F.; Wu, W.; Chen, S.H.; Wang, Z.C.; Zhu, Y.; Jiang, H.R.; Chen, R.Z.; Cheng, N.C. Compressed Ru skin on atomic-ordered hexagonal Ru-Ni enabling rapid Volmer-Tafel kinetics for efficient alkaline hydrogen evolution. *Chem. Eng. J.* **2024**, *487*, 150457. [CrossRef]
70. Wang, L.; Liu, Y.N.; Chen, Z.F.; Dai, Q.Z.; Dong, C.L.; Yang, B.; Li, Z.J.; Hu, X.B.; Lei, L.C.; Hou, Y. Theory-guided design of electron-deficient ruthenium cluster for ampere-level current density electrochemical hydrogen evolution. *Nano Energy* **2023**, *115*, 108694. [CrossRef]
71. Liu, X.; Zhang, S.Y.; Liang, J.S.; Li, S.Z.; Shi, H.; Liu, J.J.; Wang, T.Y.; Han, J.T.; Li, Q. Protrusion-rich Cu@NiRu core@shell nanotubes for efficient alkaline hydrogen evolution electrocatalysis. *Small* **2022**, *18*, 2202496. [CrossRef] [PubMed]
72. Ren, J.T.; Wang, L.; Chen, L.; Song, X.L.; Kong, Q.H.; Wang, H.Y.; Yuan, Z.Y. Interface metal oxides regulating electronic state around nickel species for efficient alkaline hydrogen electrocatalysis. *Small* **2023**, *19*, 2206196. [CrossRef] [PubMed]
73. Peng, L.S.; Zheng, X.Q.; Li, L.; Zhang, L.; Yang, N.; Xiong, K.; Chen, H.M.; Li, J.; Wei, Z.D. Chimney effect of the interface in metal oxide/metal composite catalysts on the hydrogen evolution reaction. *Appl. Catal. B Environ.* **2019**, *245*, 122–129. [CrossRef]
74. Dang, Y.L.; Wu, T.L.; Tan, H.Y.; Wang, J.L.; Cui, C.; Kerns, P.; Zhao, W.; Posada, L.; Wen, L.Y.; Suib, S.L. Partially reduced Ru/RuO_2 composites as efficient and pH-universal electrocatalysts for hydrogen evolution. *Energy Environ. Sci.* **2021**, *14*, 5433–5443. [CrossRef]
75. Li, Y.P.; Wang, W.T.; Cheng, M.Y.; Feng, Y.F.; Han, X.; Qian, Q.Z.; Zhu, Y.; Zhang, G.Q. Arming Ru with oxygen-vacancy-enriched RuO_2 sub-nanometer skin activates superior bifunctionality for pH-universal overall water splitting. *Adv. Mater.* **2023**, *35*, 2206351. [CrossRef]
76. Chen, J.L.; Feng, S.Y.; Lu, C.J.; Huang, F.J. Janus Ru/RuO_2 nano-boomerangs on carbon as pH-universal electrocatalysts with bifunctional activity toward the hydrogen/oxygen evolution reaction. *Chem. Eng. J.* **2023**, *468*, 143761. [CrossRef]
77. Zhang, H.J.; Li, X.P.; Hähnel, A.; Naumann, V.; Lin, C.; Azimi, S.; Schweizer, S.L.; Maijenburg, A.W.; Wehrspohn, R.B. Bifunctional heterostructure assembly of NiFe LDH nanosheets on NiCoP nanowires for highly efficient and stable overall water splitting. *Adv. Funct. Mater.* **2018**, *28*, 1706847. [CrossRef]
78. Lin, J.J.; Chen, J.; Tan, C.H.; Zhang, Y.Z.; Li, Y.C. Ruthenium-doped $Ni(OH)_2$ to enhance the activity of methanol oxidation reaction and promote the efficiency of hydrogen production. *RSC Adv.* **2024**, *14*, 18695–18702. [CrossRef]
79. Liu, H.B.; Jia, Q.H.; Huang, S.Q.; Yang, L.; Wang, S.T.; Zheng, L.R.; Cao, D.P. Ultra-small Ru nanoparticles embedded on Fe–$Ni(OH)_2$ nanosheets for efficient water splitting at a large current density with long-term stability of 680 hours. *J. Mater. Chem. A* **2022**, *10*, 4817–4824. [CrossRef]
80. Mo, Y.F.; Du, D.D.; Du, Y.Y.; Feng, Y.J.; Tang, P.G.; Li, D.Q. Fe $(OH)_x$ modified ultra-small Ru nanoparticles for highly efficient hydrogen evolution reaction and its application in water splitting. *J. Colloid Interf. Sci.* **2024**, *659*, 697–706. [CrossRef]
81. Anantharaj, S. Hydrogen evolution reaction on Pt and Ru in alkali with volmer-step promotors and electronic structure modulators. *Curr. Opin. Electrochem.* **2022**, *33*, 100961. [CrossRef]

82. Li, D.H.; Cai, R.S.; Zheng, D.Y.; Ren, J.; Dong, C.L.; Huang, Y.C.; Haigh, S.J.; Liu, X.E.; Gong, F.L.; Liu, Y.M.; et al. A sustainable route to ruthenium phosphide (RuP)/Ru heterostructures with electron-shuttling of interfacial Ru for efficient hydrogen evolution. *Adv. Sci.* **2024**, *11*, 2309869. [CrossRef]
83. Li, P.; Li, W.Q.; Zhao, S.E.; Huang, T.Q.; Tian, S.H.; Huang, X.F. Advanced hydrogen evolution electrocatalysis enabled by ruthenium phosphide with tailored hydrogen binding strength via interfacial electronic interaction. *Chem. Eng. J.* **2022**, *429*, 132557. [CrossRef]
84. Zhou, S.Z.; Jang, H.; Qin, Q.; Hou, L.Q.; Kim, M.G.; Liu, S.G.; Liu, X.E.; Cho, J. Boosting hydrogen evolution reaction by phase engineering and phosphorus doping on Ru/P-TiO_2. *Angew. Chem. Int. Ed.* **2022**, *61*, e202212196. [CrossRef]
85. El-Refaei, S.M.; Russo, P.A.; Schultz, T.; Chen, Z.N.; Amsalem, P.; Koch, N.; Pinna, N. Activating Ru in the pyramidal sites of Ru_2P-type structures with earth-abundant transition metals for achieving extremely high HER activity while minimizing noble metal content. *Carbon Energy* **2024**, e556. [CrossRef]
86. Li, J.; Miró, R.; Wrzesińska-Lashkova, A.; Yu, J.; Arbiol, J.; Vaynzof, Y.; Shavel, A.; Lesnyak, V. Aqueous room-temperature synthesis of transition metal dichalcogenide nanoparticles: A sustainable route to efficient hydrogen evolution. *Adv. Funct. Mater.* **2024**, 2404565. [CrossRef]
87. Pinto, F.M.; de Conti, M.C.M.D.; Pereira, W.S.; Sczancoski, J.C.; Medina, M.; Corradini, P.G.; de Brito, J.F.; Nogueira, A.E.; Góes, M.S.; Ferreira, O.P.; et al. Recent advances in layered MX_2-based materials (M = Mo, W and X = S, Se, Te) for emerging optoelectronic and photo (electro) catalytic applications. *Catalysts* **2024**, *14*, 388. [CrossRef]
88. Xu, C.Y.; Yu, H.Z.; Huang, H.M.; Huang, W.C.; Li, S.; Cao, Y.H.; Lu, H.F.; Li, G.M.; Li, Y.J.; Li, X.K.; et al. Boosting electrocatalytic activity of Ru for hydrogen evolution through engineering Ru on multiple interfaces of 1T-MoS_2 and carbon. *Chem. Eng. J.* **2024**, *489*, 151295. [CrossRef]
89. Zhang, X.; Zhou, F.; Zhang, S.; Liang, Y.Y.; Wang, R.H. Engineering MoS_2 basal planes for hydrogen evolution via synergistic ruthenium doping and nanocarbon hybridization. *Adv. Sci.* **2019**, *6*, 1900090. [CrossRef]
90. Islam, S.E.; Hang, D.R.; Liang, C.T.; Sharma, K.H.; Huang, H.C.; Chou, M.M.C. Tuning the electrocatalytic activity of MoS_2 nanosheets via the in situ hybridization with ruthenium and graphene network. *Chem. Eng. J.* **2024**, *488*, 150950. [CrossRef]
91. Li, X.H.; Han, S.H.; Qiao, Z.L.; Zeng, X.F.; Cao, D.P.; Chen, J.F. Ru monolayer island doped MoS_2 catalysts for efficient hydrogen evolution reaction. *Chem. Eng. J.* **2023**, *453*, 139803. [CrossRef]
92. Cai, J.L.; Ding, J.; Wei, D.H.; Xie, X.; Li, B.J.; Lu, S.Y.; Zhang, J.M.; Liu, Y.S.; Cai, Q.; Zang, S.Q. Coupling of Ru and O-vacancy on 2D Mo-based electrocatalyst via a solid-phase interface reaction strategy for hydrogen evolution reaction. *Adv. Energy Mater.* **2021**, *11*, 2100141. [CrossRef]
93. Zhao, J.J.; Guo, Y.N.; Li, S.J.; Wang, J.Q.; Liu, K.H.; Dai, L.J.; Dai, Y.; Jiang, B.; Li, H.X. Amorphous-crystalline porous ruthenium selenide as highly efficient electrocatalysts for alkaline hydrogen evolution. *Chem. Eng. J.* **2024**, *485*, 150074. [CrossRef]
94. Kuang, Y.B.; Yang, F.L.; Feng, L.G. Advancements in ruthenium (Ru)-based heterostructure catalysts: Overcoming bottlenecks in catalysis for hydrogen evolution reaction. *Adv. Energy Mater.* **2024**, *14*, 2402043. [CrossRef]
95. Bae, S.Y.; Mahmood, J.; Jeon, I.Y.; Baek, J.B. Recent advances in ruthenium-based electrocatalysts for the hydrogen evolution reaction. *Nanoscale Horiz.* **2020**, *5*, 43–56. [CrossRef]
96. Li, Y.Q.; Liu, X.; Xu, J.L.; Chen, S.R. Ruthenium-based electrocatalysts for hydrogen evolution reaction: From nanoparticles to single atoms. *Small* **2024**, 2402846. [CrossRef]
97. Song, J.T.; Qian, Z.X.; Yang, J.; Lin, X.M.; Xu, Q.C.; Li, J.F. In situ/operando investigation for heterogeneous electro-catalysts: From model catalysts to state-of-the-art catalysts. *ACS Energy Lett.* **2024**, *9*, 4414–4440. [CrossRef]
98. Sun, Y.L.; Deng, Y.L.; Chen, H.N.; Yang, X.T.; Lin, X.M.; Li, J.F. Design strategies and in situ infrared, Raman, and X-ray absorption spectroscopy techniques insight into the electrocatalysts of hydrogen energy system. *Small Struct.* **2023**, *4*, 2200201. [CrossRef]
99. Lin, X.M.; Li, J.F. Applications of in situ Raman spectroscopy on rechargeable batteries and hydrogen energy systems. *ChemElectroChem* **2023**, *10*, e202201003. [CrossRef]

Disclaimer/Publisher's Note: The statements, opinions and data contained in all publications are solely those of the individual author(s) and contributor(s) and not of MDPI and/or the editor(s). MDPI and/or the editor(s) disclaim responsibility for any injury to people or property resulting from any ideas, methods, instructions or products referred to in the content.